DOE/ER/13262--9

DE93 007306

A progress report

for the period Jan. 1, 1990 to Dec. 1, 1992

Grant DE-FG05-84ER13262

EXCITATION OF ATOMS AND MOLECULES IN COLLISIONS WITH HIGHLY CHARGED IONS

Submitted by the

Cyclotron Institute

Texas A&M University

College Station, TX 77843

to the

Fundamental Interactions Branch

Division of Chemical Sciences

Office of Basic Energy Sciences

U.S. Department of Energy

Principal Investigator

Rand L. Watson, Professor of Chemistry

January 1, 1993

TABLE OF CONTENTS

DISCLAIMER

I. INTRODUCTION

This report summarizes progress in research supported by DOE Grant DE-FG05-84ER13262 during the period January 1, 1990 to December 1, 1992. Contained herein are the titles of publications and presentations which have evolved from completed projects, and the titles of papers which have been submitted for publication. Summaries of work that has not yet been published constitute the main body of this report, while the appendix contains reprints of all publications produced during the present grant period.

II. OVERVIEW OF COMPLETED WORK

A study of the double ionization of He by high energy N^{7+} ions, which began during the previous grant period, was extended up in energy to 40 MeV/amu. These measurements verified the deviations from the predictions of the forced-impulse-approximation theory observed in our previous work and indicated that the energy required to reach the limiting value of the ratio of double-to-single ionization cross sections may be as high as 70 MeV/amu.

Coincidence time-of-flight studies of multicharged N_2, O_2, and CO molecular ions produced in collisions with 97 MeV Ar^{14+} ions, which constituted the dissertation project of Gabriel Sampoll, were completed. The work on carbon monoxide was particularly illuminating since dissociation channels leading to ion-pairs in which each partner had the same charge were detectable for this heteronuclear molecule. Dissociation products from transient CO^{Q+}, where Q ranged from 2 to 7, were identified by coincidence time-of-flight spectroscopy in which the

time-of-flight of the first ion to reach the detector and the time difference between the first ion and its partner were recorded event-by event. An iterative matrix transformation procedure was employed to convert the time-difference spectra for the prominent dissociation channels into total kinetic energy distributions.

Analysis of the total kinetic energy distributions and comparisons with the available data for CO^{2+} and CO^{3+} from synchrotron radiation experiments led to the conclusion that ionization by Ar-ion impact populates states having considerably higher excitation energies than those accessed by photoionization. The average excitation energy produced in Ar-ion collisions increases by approximately 78 eV per electron removed from the CO molecule for charges of 3+ and above. It was found that the average total kinetic energy released in the dissociation of molecular ions produced by Ar-ion impact is systematically greater than that predicted by a simple point-charge model. This result is somewhat puzzling in view of the few theoretical results available which tend to indicate that the point-charge Coulomb potential lies above most of the states connecting to low-energy asymptotic configurations. This observation may indicate that most of the dissociation channels populated in Ar-ion collisions lead to highly excited product ions.

The dissociation fractions for CO^{1+} and CO^{2+} molecular ions, and the branching ratios for the most prominent charge division channels of CO^{2+} through CO^{7+} were determined from time-of-flight singles and coincidence data. The characteristics of the dissociation fractions and yield ratios for CO^{1+} and CO^{2+} produced in 97-MeV Ar^{14+} collisions

were found to be similar to those observed for low energy H^+ and He^{2+} projectiles in the same perturbative regime relative to the CO valence electrons. An analysis of the ion-pair production yields revealed a preference for symmetric or near-symmetric charge division channels, more or less in accordance with expectations based on the minimum excitation energies required for their production. The observation of an enhancement in the ionization probabilities of CO for high Q over those obtained for Ne suggested that electron transfer during the early stages of the dissociation process followed by LMM Auger decay plays an important role in determining the final charges of the dissociation products.

An experiment designed to investigate the orientation dependence of dissociative multielectron ionization of molecules by heavy ion impact was completed. These measurements, which employed a gas jet, an ion collection field, and a 2-dimensional position sensitive microchannel plate detector, revealed that anisotropies resulting from the dissociation of N_2 molecular ions produced by pure-ionization-collisions of 97 MeV Ar^{14+} ions are too weak to be accurately determined by this detection method. A new detection system for measuring the positions of both ions from binary dissociation events has been designed and is currently being tested. This system employs a CCD camera interfaced to an IBM PC compatible computer through a special video card. The video card provides a digital readout of the video intensity as a function of the x and y coordinates, thereby giving a numerical reproduction of the video display. By using the CCD camera system in conjunction with a large MCP backed by a phosphorescent screen to determine ion positions

in coincidence with their flight times, the three-dimensional velocity vectors of both dissociation products from individual dissociation events can be constructed. We plan to perform these experiments during the next grant period.

Measurements of the cross sections for K-shell ionization of intermediate Z elements by 30-MeV/amu H, N, Ne, and Ar ions were completed. The cross sections were determined for solid targets of Z = 13, 22, 26, 29, 32, 40, 42, 46, and 50 by recording the spectra of K x-rays with a Si(Li) spectrometer in coincidence with beam particles detected in a microchannel plate assembly. Most of the collision systems investigated lie outside the region of proven validity of the ECPSSR formulation, which ranges from Z_1/Z_2 = 0.03 to 0.3 and v_1/v_K = 0.07 to 2 (where v_1 is the projectile velocity and v_K is the average K-electron velocity of the target). Overall, the experimental cross sections displayed good agreement with the cross sections calculated using the ECPSSR theoretical formulation. The largest deviations between the experimental and calculated cross sections were of the order of 20% and occurred for Ar projectiles incident on targets with Z from 26 to 40. It was concluded that these deviations are probably attributable to the fact that, on average, the Ar projectiles were not fully stripped of their electrons. This would cause the capture contribution to the total K-shell ionization cross section to be smaller than predicted by the ECPSSR calculations.

III. PERSONNEL

R. L. Watson	-Professor, Department of Chemistry and Cyclotron Institute (Principal Investigator)
K. Wohrer	-Visiting Scientist from Institut Curie, Paris, France (Sept., 1990 to Sept., 1991)
O. Heber	-Research Collaborator from the Weizmann Institute, Rehovot Israel
V. Horvat	-Postdoctoral Research Associate (through May, 1992) and Assistant Research Scientist (since June, 1992)
M. Chabot	-Postdoctoral Research Associate (Sept., 1990 to Sept, 1991)
G. Sampoll	-Graduate Research Assistant (through Dec., 1991) and Postdoctoral Research Associate (since Jan., 1992)
R. Parameswaren	-Postdoctoral Research Associate (since Oct., 1991)
N. Matutina	-Graduate Research Assistant (Sept., 1990 through May, 1990)
S. Wu	-Graduate Student (Sept., 1991 through Feb., 1992)
B. Hill	-Undergraduate Research Assistant (through Aug., 1991)
T. Lotze	-Undergraduate Research Assistant (through Aug., 1991)
M. Barrett	-Undergraduate Research Assistant (through May, 1992)
B. Griffith	-Undergraduate Research Assistant (through May, 1992)
N. Peffer	-Undergraduate Student (June, 1992 through Aug., 1992)
L. Cook	-Undergraduate Student (since Nov., 1992)

IV. PUBLICATIONS AND PRESENTATIONS

A. Publications

O. Heber, G. Sampoll, B. B. Bandong, and R. L. Watson, "Charge Distributions of Ar Recoil-Ions Produced in One- and Two-Electron Capture Collisions by 16 MeV O^{q+} Projectiles," Phys. Rev. A40, 5601-5604 (1989).

O. Heber, B. B. Bandong, G. Sampoll, and R. L. Watson, "Double and Single Ionization of Helium by High-Velocity N^{7+} Ions," Phys. Rev. Lett. 64, 851-853 (1990).

O. Heber, R. L. Watson, G. Sampoll, and B. B. Bandong, "Three-Shell Model for Independent-Electron Processes in Heavy-Ion-Atom Collisions," Phys. Rev. A42, 6466-6470 (1990).

O. Heber, "K-Shell Vacancy Production by Direct Coulomb Ionization in 47-MeV Ca^{17+} + Ar Collisions," Phys. Rev. A42, 1795-1798 (1990).

R. L. Watson, D. A. Church, R. E. Tribble, L. Yang, B. B. Bandong, and T. Lotze, "Atomic Physics with the Texas A&M ECR Ion Source," Nucl. Instr. and Meth. B56, 223-226 (1991).

O. Heber, R. L. Watson, and G. Sampoll, "Recoil-Ion Kinetic Energies for 96 MeV Ar Collisions, "Nucl. Instr. and Meth. B56, 232-234 (1991).

O. Heber, R. L. Watson, G. Sampoll, V. Horvat, B. Hill, and T. Lotze, "Multiple Ionization of He, Ne, and Ar by High Velocity N^{7+} Ions," Nucl. Instr. and Meth. B56, 15-17 (1991).

V. Horvat, R. L. Watson, G. Sampoll, T. Lotze, and B. Hill, K- plus L-shell Ionization of 4th Row Elements by 30 MeV/amu Ar Ions," Nucl. Instr. and Meth. B56, 61-62 (1991).

G. Sampoll, R. L. Watson, O. Heber, V. Horvat, K. Wohrer, and M. Chabot, "Dissociation of Multicharged CO Molecular Ions Produced in Collisions with 97 MeV Ar^{14+}: Total Kinetic Energy Distributions," Phys. Rev. A45, 2903-2914 (1992).

V. Horvat, G. Sampoll, K. Wohrer, M. Chabot, and R. L. Watson, "K-Shell Ionization of Intermediate Z Elements by 30-MeV/amu H, N, Ne, and Ar Ions," Phys. Rev. A46, 2572-2580 (1992).

K. Wohrer, G. Sampoll, R. L. Watson, M. Chabot, O. Heber, and V. Horvat, "Dissociation of Multicharged CO Molecular Ions Produced in Collisions with 97 MeV Ar^{14+}: Dissociation Fractions and Branching Ratios," Phys. Rev. A46, 3929-3934 (1992).

B. M. Hill, R. L. Watson, K. Wohrer, B. B. Bandong, G. Sampoll, and V. Horvat, "Ionization of Noble Gas Atoms by Alpha Particles and Fission Fragments from the Decay of ^{252}Cf," Int. J. Mass Spect. and Ion Proc. (in press).

B. Dissertations

"Double Coincidence Studies of Molecular Dissociation Induced by Heavy Ion Impact," Gabriel Sampoll Ramirez, December, 1991.

C. Invited Presentations

Ionization of Atoms and Small Molecules in Fast Heavy Ion Collisions, R. L. Watson, Twelfth International conference on the Application of Accelerators in Research and Industry, Denton, Texas, Nov. 2-5, 1992.

Multiple Ionization of Atoms and Small Molecules by Fission Fragments and Other Fast Ions, R. L. Watson, Texas Symposium on Mass Spectrometry VI; ^{252}Cf-Plasma Desorption Mass Spectrometry, Gaspe, Quebec, Canada, May 15-19, 1992.

Dissociation of Multicharged CO Molecular Ions Produced in Collisions with 97 MeV Ar^{14+}, Twelfth DOE Atomic Physics Program Workshop, Kansas State University, Manhattan KS, October 15-16, 1991.

Multicharged Recoil-Ion Production in Ion-Atom Collisions, R. L. Watson, Oak Ridge National Laboratory, Oak Ridge, TN, (March 26, 1990).

D. Contributed Presentations

Multiple Ionization of Noble Gases in Electron Capture and Loss Collisions by 8 MeV/amu Kr^{32+} and Kr^{13+} Collisions, R. Parameswaren, G. Sampoll, V. Horvat, and R. L. Watson, Twelfth International conference on the Application of Accelerators in Research and Industry, Denton, Texas, Nov. 2-5, 1992.

Probability of Dissociation and Main Dissociative Pathways of CO Molecular Ions Produced in Collisions with 97 MeV Ar^{14+} Projectiles, M. Chabot, O. Heber, G. Sampoll, R. L. Watson, and K. Wohrer, Second International Symposium on Swift Heavy Ions in Matter, Bensheim, Germany, May 19-22, 1992.

Coulomb Explosions of Diatomic Molecules Following Multiple Ionization by Fast Heavy Ion Impact, G. Sampoll, O. Heber, M. Chabot, K. Wohrer, and R. L. Watson, 17th International Conference on the Physics of Electronic and Atomic Collisions, Brisbane, Australia, July 10-16, 1991.

K-Shell Ionization by 30 MeV/amu Heavy Ions, V. Horvat, G. Sampoll, M. Chabot, K. Wohrer, and R. L. Watson, 17th International Conference on the Physics of Electronic and Atomic Collisions, Brisbane, Australia, July 10-16, 1991.

Resonant Dielectronic Excitation of Ti Ions in a Crystal Channel, P. F. Dittner, S. Datz, R. Vane, H. F. Krause, J. Gomez Del Campo, R. Watson, P. Ziejlmans van Emmichoven, and U. Bechthold, 21st Annual Meeting of the Division of Atomic, Molecular, and Optical Physics, American Physical Society, Monterey, CA (May 21-23, 1990); Bull. Am. Phys. Soc. 35, 1160 (1990).

Z-Dependence of K-Shell Ionization at 30 MeV/amu, V. Horvat, R. L. Watson, G. Sampoll, and T. Lotze, Eleventh Conference on the Application of accelerators in Research and Industry, Denton, TX, November 5-8, 1990; Bull. Am. Phys. Soc.35, 1713 (1990).

Dissociation of Multicharged Molecular Ions Produced in Collisions with 97 MeV Ar^{14+}, G. Sampoll, R. L. Watson, O. Heber, and V. Horvat, Eleventh Conference on the Application of accelerators in Research and Industry, Denton, TX, November 5-8, 1990; Bull. Am. Phys. Soc.35, 1719 (1990).

Multicharged Recoil-Ion Production by ^{252}Cf Fission Fragments, B. Hill, R. L. Watson, B. B. Bandong, and G. Sampoll, Eleventh Conference on the Application of accelerators in Research and Industry, Denton, TX, November 5-8, 1990; Bull. Am. Phys. Soc.35, 1719 (1990).

Recoil-Ion Kinetic Energies for Collisions of 96 MeV Ar, O. Heber, R. L. Watson, G. Sampol, and B. B. Bandong, Eleventh Conference on the Application of accelerators in Research and Industry, Denton, TX, November 5-8, 1990; Bull. Am. Phys. Soc.35, 1720 (1990).

V. PROJECT REPORTS

A. Dissociation of Highly Charged CO Molecular Ions Produced in Electron Capture Collisions of 97 MeV Ar^{14+}

(G. Sampoll, R. L. Watson, V. Horvat, M. Barrett, and B. Griffith)

Electron capture collisions occur at much smaller impact parameters, on average, than collisions in which the charge of the projectile remains unchanged. The so-called transfer ionization (TI) process, in which electron capture to the projectile is accompanied by additional Coulomb ionization of the target, leads to an enhancement of the higher charge states of the target relative to the charge state distribution typically produced by pure ionization (PI) collisions. This property has been utilized recently in an experiment designed to investigate the dissociation of highly charged CO molecular ions.

The experiment was performed using the same differentially pumped gas cell system described in Ref. [1]. A time-of-flight (TOF) spectrometer was employed to measure the TOF of the first dissociation product ion to reach the microchannel plate (MCP) detector and the flight time difference between the first ion and its dissociation partner in coincidence with 97 MeV Ar^{14+} projectiles. The TOF spectrometer consisted of two acceleration stages identical to those described in [1], and a modified 2.5-cm diameter flight tube 15-cm in length attached to a 2-cm diameter chevron MCP detector. Behind the gas cell was placed a projectile charge state analyzer which consisted of a bending magnet and a one-dimensional position sensitive MCP (1 x 4-cm). The three parameter data were acquired on a MICROVAX II computer using

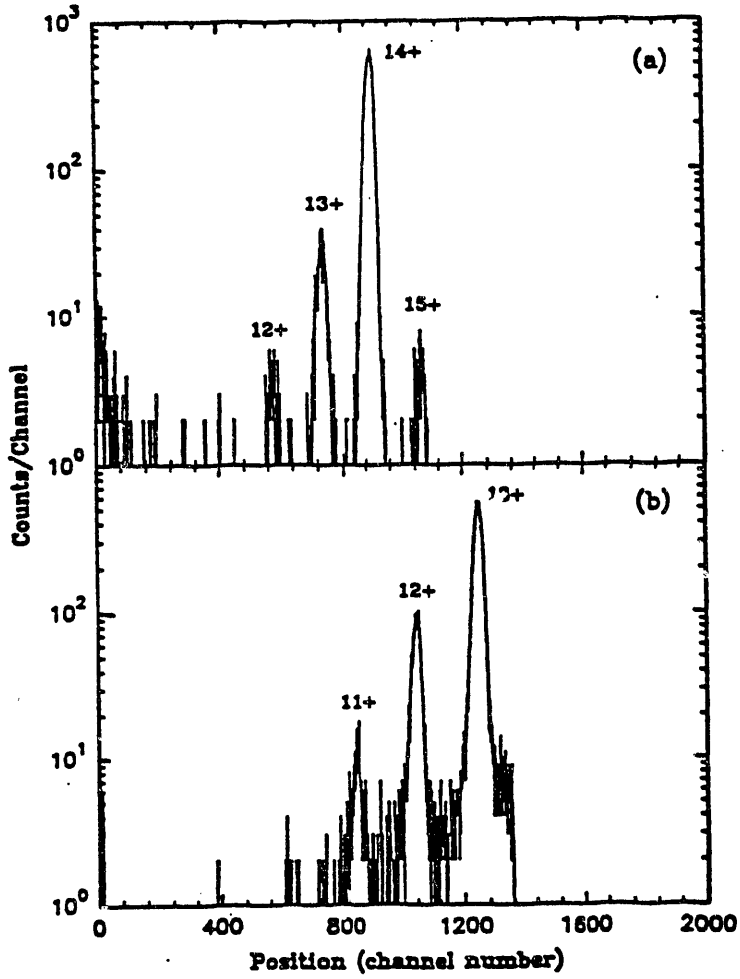

Figure 1. Position spectra showing the charge state distribution of the Ar^{14+} projectiles after passing through the gas cell taken (a) without and (b) with the detector mask.

the Los Alamos Q-system software and recorded on magnetic tape event-by-event. The position spectrum showing the charge state distribution of the Ar^{14+} projectiles after passing through the gas cell is presented in Figure 1 (a). In order to increase the counting rate for electron capture collisions, projectiles with exit charge states $\geq$ 14+ were prevented from hitting the position sensitive MCP by a mask during part of the run. The resulting position spectrum is shown in Figure 1 (b).

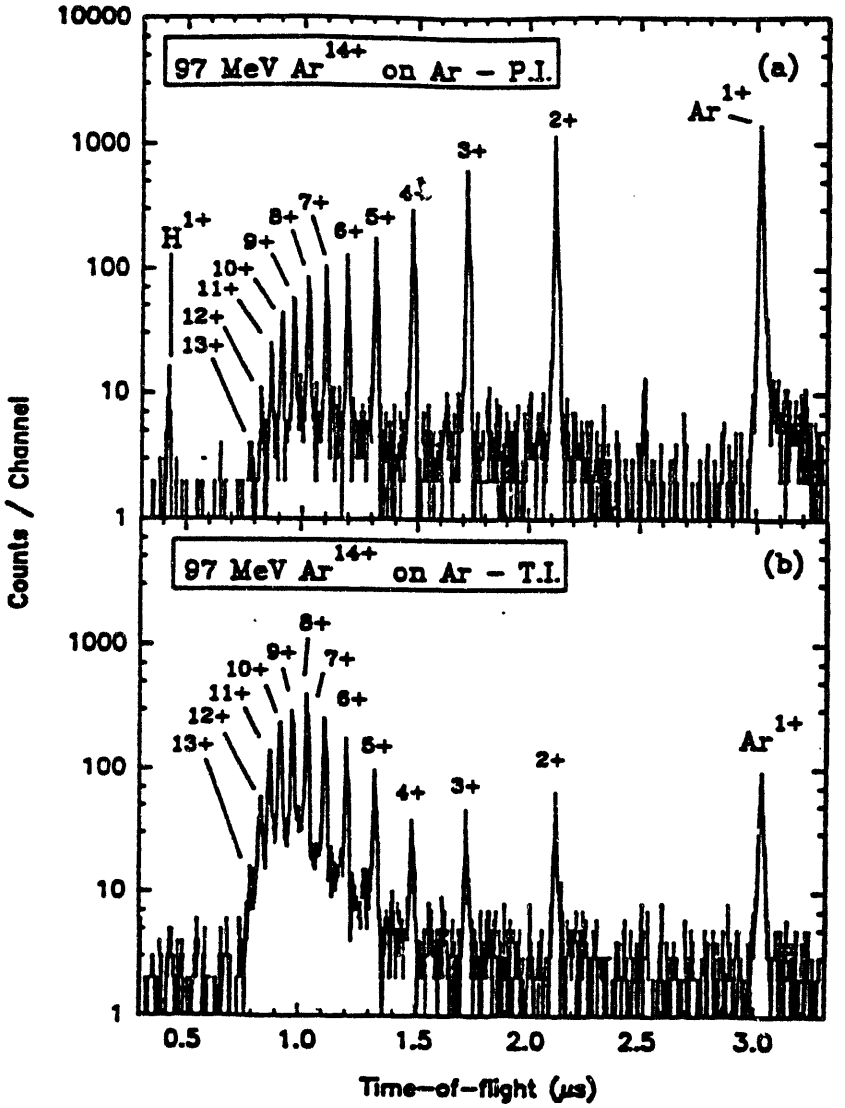

Figure 2. Time-of-flight spectrum of Ar ions produced by (a) pure ionization (PI) and (b) transfer ionization (TI) collisions of 97 MeV Ar^{14+} with Ar.

Calibration of the TOF spectrometer $(M/q)^{1/2}$ scale (where M and q are respectively the ion's mass and charge) was accomplished by measuring TOF spectra for an Ar target gas. The spectra obtained for charge unchanged (PI) collisions and electron capture collisions (TI) are shown in Figures 2 (a) and (b). From these spectra, it is apparent that charge states up to 13+ are produced for this collision system. In the TI spectrum [Figure 2(b)], the charge states in the vicinity of 8+

are greatly enhanced relative to the low charge states. In fact, the yields of Ar^{1+}, Ar^{2+}, and Ar^{3+} in this spectrum are almost entirely attributable to PI collisions of projectiles that had captured an electron prior to entering the gas cell. The ratio of Ar^{13+} to Ar^{14+} in the incident beam was found to be 2.0×10^{-2}.

A two-dimensional display of the TOF versus time-difference data obtained for ions produced in electron capture collisions of 97 MeV Ar^{14+} with CO molecules is shown in Figure 3(a). Projection of this data onto the TOF axis gives the first-ion TOF spectrum shown in Figure

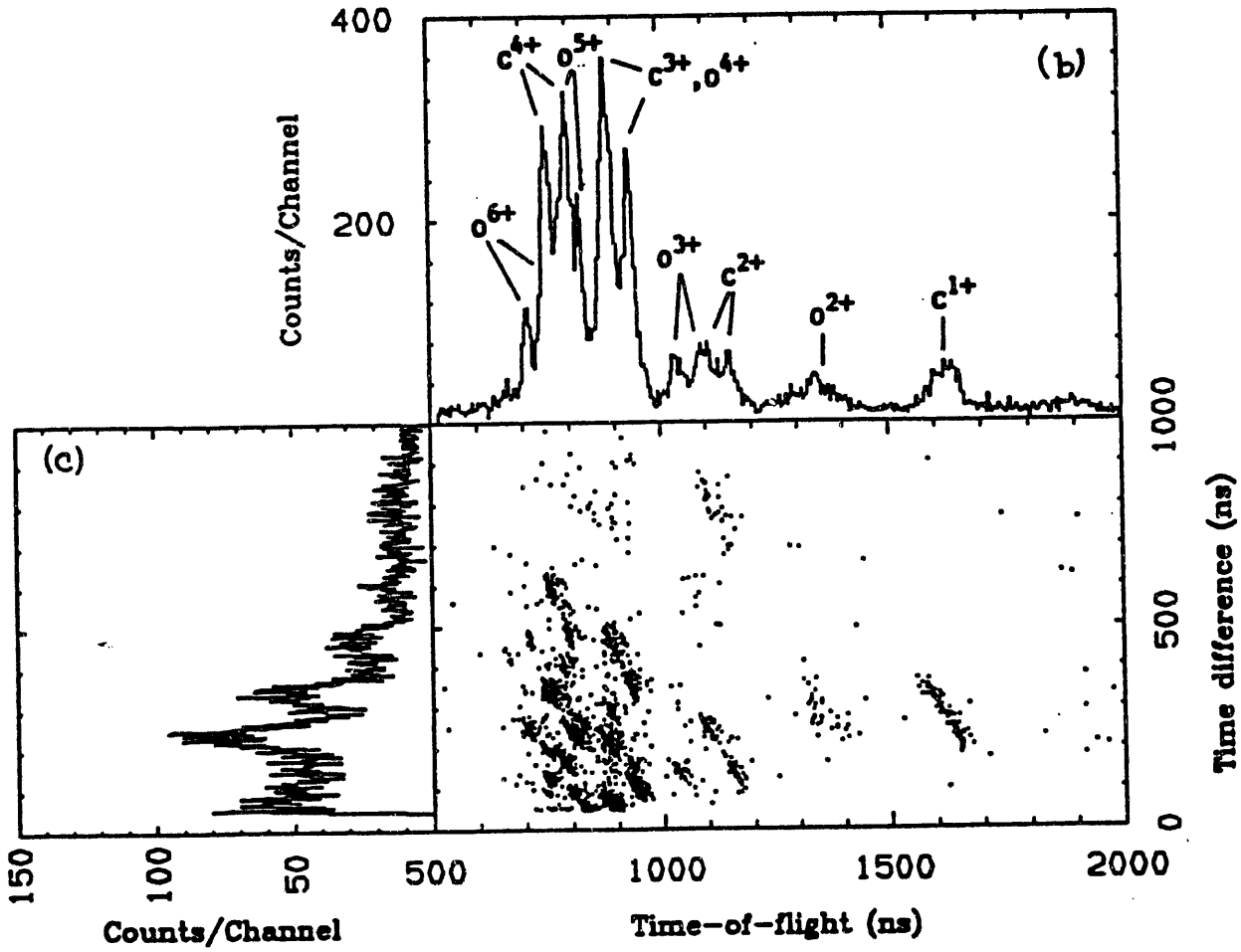

Figure 3. Two-dimensional display of the data for CO dissociation product ions produced in electron capture collisions.

3(b), while projection onto the time-difference axis gives the total ion-pair time-difference spectrum shown in Figure 3(c). Comparison of the first-ion TOF spectrum with that obtained for pure-ionization collisions (see Ref. [1]) confirms the prediction that in TI collisions with molecules the higher charge states are greatly enhanced relative to the distribution of ions resulting from PI collisions. Nevertheless, it is apparent that the highest charge observed for C-ions is 4+ and the highest charge observed for O-ions is 6+, implying that even though a K-vacancy is produced in these capture collisions, it does not survive during the relaxation process that follows.

By placing windows around each of the two-dimensional data "islands" appearing in Figure 3(a) and projecting only events within these islands onto the time-difference axis, separate ion-pair time-difference distributions were obtained for each of the statistically significant dissociation channels within the observation range of the experiment. The various ion-pair time-difference distributions associated with electron capture collisions are shown in Figures 4 and 5. The time consuming process of transforming these time-difference distributions into total kinetic energy distributions is currently in progress. The goal of this effort is to compare the average total kinetic energies for specific dissociation channels excited in PI, one-electron TI, and two-electron TI to see if the excitation energies of the parent molecular ions are significantly different.

REFERENCES

[1] G. Sampoll, R. L. Watson, O. Heber, H. Horvat, K. Wohrer, and M. Chabot, Phys. Rev. A 45, 2903 (1992).

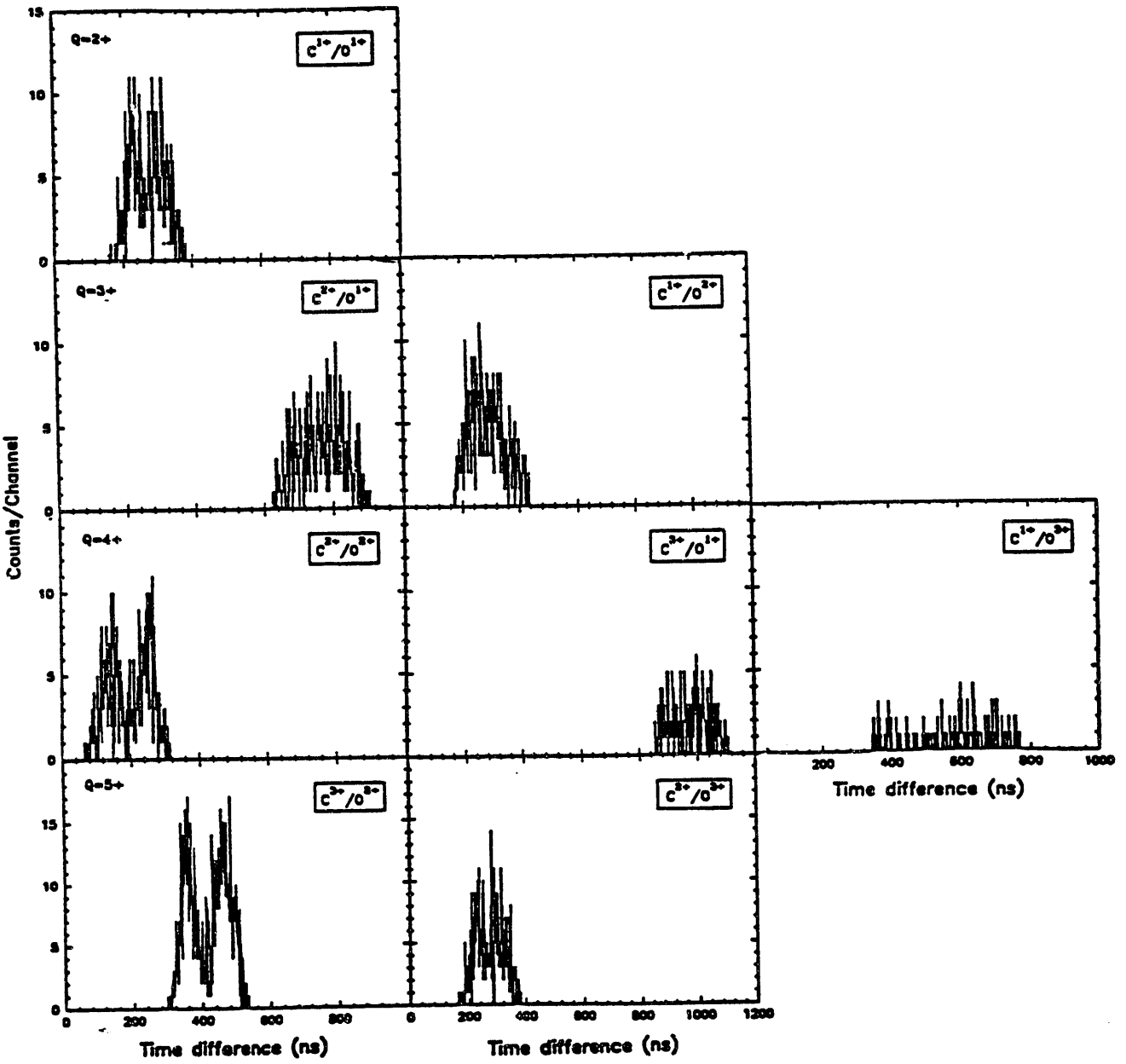

Figure 4. Sorted ion-pair time-difference distributions for the statistically significant dissociation channels of CO^{Q+} molecular ions produced in electron capture collisions by 97 MeV Ar^{14+}, where Q = 2 to 5.

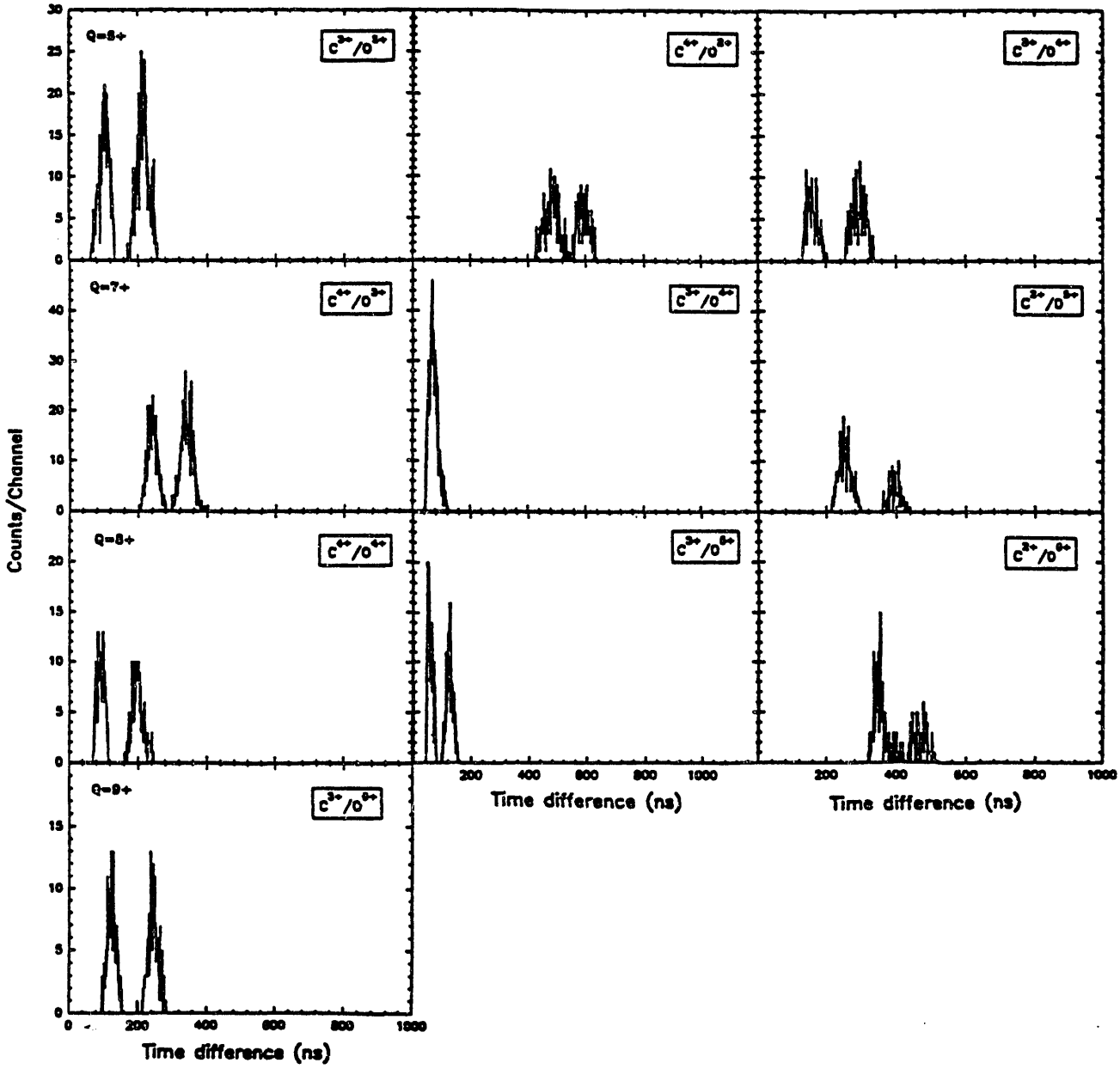

Figure 5. Sorted ion-pair time-difference distributions for the statistically significant dissociation channels of CO^{Q+} molecular ions produced in electron capture collisions by 97 MeV Ar^{14+}, where Q = 6 to 9.

B. Model Calculations of Multielectron Ionization of Diatomic Molecules by Heavy-Ion Impact (K. Wohrer and R. L. Watson)

In order to estimate the magnitude of geometrical effects on the ionization of diatomic molecules by heavy-ion impact, a simple model was developed for calculating multiple ionization cross sections in the two limiting cases of parallel and perpendicular orientation of the internuclear axis relative to the beam axis. The model is based upon the assumptions that (a) the molecule is composed of independent atoms whose electron distributions are the same as those of separated atoms, and (b) the ionization cross sections may be calculated using the independent electron approximation (IEA). The first assumption obviously ignores the fact that strongly bonded systems, such as N_2 and CO (bond order = 3) and O_2 (bond order = 2), have electron distributions that are quite different than just the sum of the overlapping electron distributions of the two individual atoms. Nevertheless, this approximation should suffice for the level of accuracy required in the present estimates. The range of validity of the second assumption is the subject of numerous studies and cannot be assessed with certainty. (Restrictions on the applicability of this approximation have been discussed by McGuire and Weaver [1]). However, the IEA has been found to work well for collisions systems similar to the ones of interest here [2]

A schematic diagram showing the relevant parameters for the parallel and perpendicular orientations is presented in Fig. 1. In the parallel orientation, the impact parameter b is defined relative to the internuclear axis of the molecule (which passes through the nuclei

of both atoms), whereas in the perpendicular orientation, the impact parameter is defined relative to an axis that is perpendicular to the internuclear axis and passes through its center. In the parallel case, the ionization probability for either atom depends only on b. Employing the IEA, the probability of removing n electrons from a shell containing N electrons may be expressed as

$$P_n(b) = \binom{N}{n} p^n(b)[1 - p(b)]^{N-n} \qquad (1)$$

where p(b) is the ionization probability for a single electron. In the perpendicular case, the ionization probability depends on both the

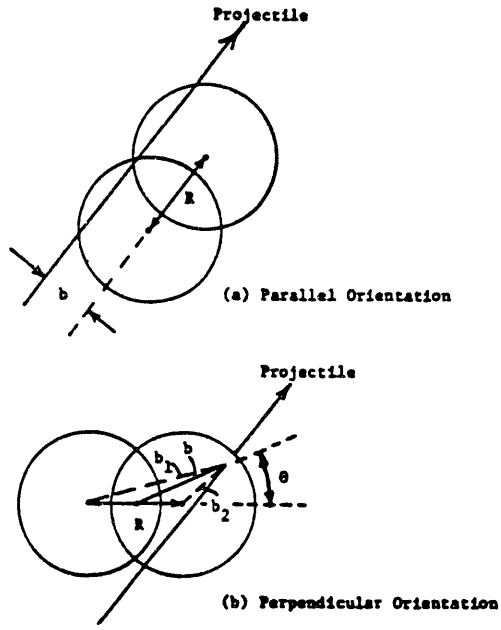

Figure 1. Schematic diagram showing the model parameters for (a) parallel and (b) perpendicular orientations.

impact parameter b and the angle θ. The probability for removing n electrons from either atom in the perpendicular orientation may be expressed in terms of the impact parameters measured relative to the individual nuclei, b_1 or b_2, as

$$P_n(b_j) = \binom{N}{n} p^n(b_j)[1 - p(b_j)]^{N-n} \qquad (2)$$

where $b_j = [b^2 + (R/2)^2 \pm bR\cos\theta]^{1/2}$ and $j = 1$ or 2. The total cross sections for removing k electrons from the molecule, where n electrons come from atom 1 and m electrons come from atom 2, are then given by

parallel orientation:

$$\sigma_k = 2\pi \int_0^\infty \sum_{n+m=k} P_n(b)P_m(b)bdb \ , \qquad (3)$$

perpendicular orientation:

$$\sigma_k = \int_0^{2\pi} \int_0^\infty \sum_{n+m=k} P_n(b_1)P_m(b_2)bdbd\theta \ . \qquad (4)$$

In the present calculations, the one-electron ionization probability was represented by the commonly used formula

$$p(b) = p_o \exp(-b/r_L) \qquad (5)$$

in which p_o is the ionization probability at zero impact parameter and r_L is a radial parameter for L-shell ionization. For the ionization of elements in the vicinity of Ne by 1 to 2 MeV/amu projectiles having ionic charges in the range of 4+ to 9+, p_o values around 0.6 and r_L values corresponding to the average L-shell radius have been found to give an adequate representation of p(b) [2].

The results presented in Fig. 2 for the ionization of O_2 molecules were calculated using $p_o = 0.4$, $r_L = 0.6$ Å, and $R = 1.2$ Å. They show that the cross sections for removing more than about 4 electrons from molecules in the parallel orientation are considerably larger than those

for the perpendicular orientation. Intuitively, this is exactly what one would expect, since the removal of large numbers of electrons requires relatively smaller impact parameters. In the parallel orientation, each trajectory passes through both atoms and therefore has two chances of removing electrons from the molecule. The results obtained for the production of low charge states ($k < 4$), show that the cross sections are only slightly larger for the perpendicular orientation than for the parallel orientation, which is somewhat surprising since one intuitively expects the molecule to present a considerably larger target in the perpendicular orientation than in the parallel orientation. Calculations performed using smaller p_o values yielded cross sections

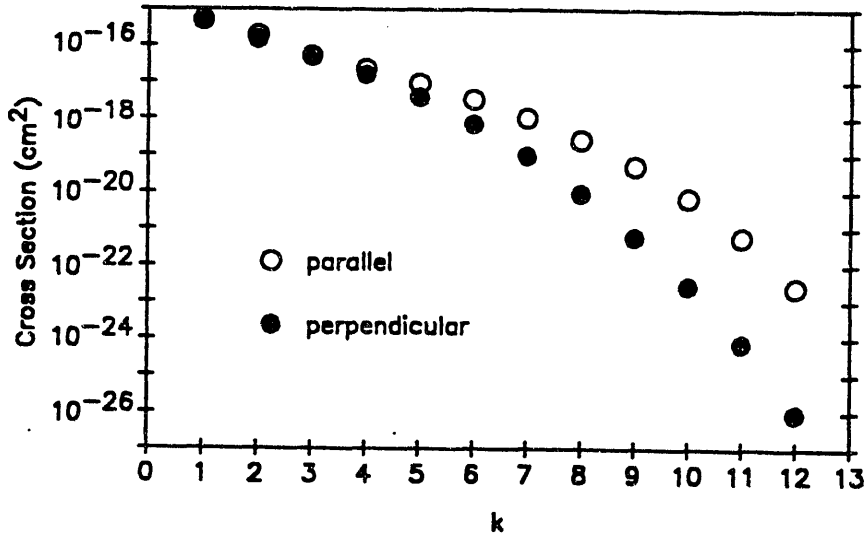

Figure 2. Calculated cross sections for the ionization of k electrons from O_2 molecules in parallel and perpendicular orientations.

that displayed a somewhat larger preference for the perpendicular orientation at low k values.

The differences between the ionization cross sections for the two orientations are greatly magnified when the radius of the shell being ionized is smaller than the internuclear separation. Cross sections calculated for K-shell ionization of O_2 (r_K = 0.1 Å) are compared in Table 1. It is evident that the cross sections for the parallel orientation are much larger than those for the perpendicular orientation for k values as low as 2.

The above results predict that geometrical effects on the ionization cross sections for H_2, for which the internuclear separation is of the same order of magnitude as the shell radius, should be very small. In the case of N_2, however, the present model predicts a significantly larger cross section for the production of highly charged recoil-ions in the parallel orientation than in the perpendicular orientation. This is in qualitative agreement with the results of Varghese et al. [3]. On the other hand, the experimentally observed preference for the perpendicular orientation in the production of N^{2+} cannot be understood in terms of the present model calculations, which predict that the cross sections for the production of low charge states are essentially independent of orientation. Moreover, Varghese et al. observed the same effect for N^{2+} recoil-ions produced in one-electron capture collisions. In this case, electron capture must occur predominately from the K-shell, but still the present calculations fail to predict an observable effect (see comparison in Table 1 for k = 1). This interesting disparity provides added motivation for further

investigations of orientation effects on the ionization cross sections for molecules.

Table 1. Calculated K-shell ionization cross sections (in units of 10^{-16} cm^2) for O_2 molecules.

Number of electrons ionized (k)	Cross section parallel orientation	perpendicular orientation
1	0.11	0.13
2	1.5×10^{-2}	7.2×10^{-3}
3	2.0×10^{-3}	1.8×10^{-10}
4	1.5×10^{-4}	9.1×10^{-18}

References

[1] J. H. McGuire and L. Weaver, Phys. Rev. A16, 41 (1977).

[2] O. Heber, G. Sampoll, B. B. Bandong, R. J. Maurer, E. Moler, R. L. Watson, I. Ben-Itzhak, J. L. Shinpaugh, J. M. Sanders, L. Hefner, and P. Richard, Phys. Rev. A9, 4898 (1989).

[3] S. L. Varghese, C. L. Cocke, S. Cheng, E. Y. Kamber, and V. Frohne, Nucl. Instr. and Meth. B40, 266 (1989).

C. Orientation Dependence of Fast-Collision-Induced Molecular Dissociation

(M. Chabot, K. Wohrer, G. Sampoll, V. Horvat, and R. L. Watson)

An experiment designed to investigate the orientation dependence of the cross section for ionization of N_2 by 97 MeV Ar^{14+} has been performed. Orientation dependent cross sections can occur as a result of interference between the scattering amplitudes associated with the different atomic centers [1], and as a result of geometrical effects [2].

A schematic diagram of the system is shown in Fig. 1. Gas was injected into the vacuum system through the 10 μm (diameter) x 500 μm holes of a microchannel plate mounted over a 1 mm diameter hole in a 0.25 mm thick brass cover plate. The input gas pressure above the microchannel plate was monitored by a capacitance manometer and maintained around 0.5 Torr. Under these conditions, the theoretical width of the jet 3 mm from the cover plate was about 2.5 mm and the theoretical maximum density of the jet at this distance was $\approx 3 \times 10^{13}$ molecules/cm^3 [3].

The gas jet was enclosed by a three-stage ion collection/time-of-flight spectrometer system. In the first stage, ions created by the dissociation of molecules induced by collisions with the heavy-ion beam passing through the jet at a distance of 2.5 mm from the cover plate were accelerated in the downward direction by a uniform electric field of nominal strength 200 V/cm between the cover plate and the first grid. Another uniform electric field of nominal strength 500 V/cm between grid 1 and grid 2 further accelerated the ions in the downward direction.

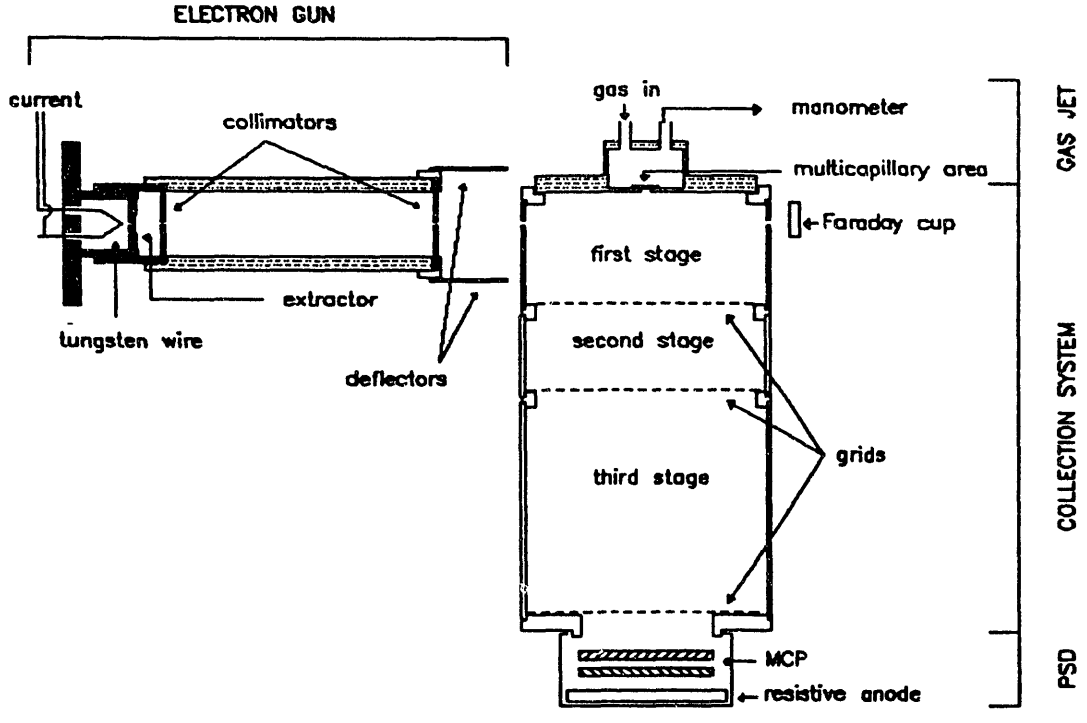

Figure 1. A schematic diagram of the gas jet and ion collection/ time-of-flight spectrometer system.

Both fields were adjusted to control the maximum drift radius of the ions in the horizontal direction and to optimize the space focusing for the time-of-flight measurements. The third stage was a field free region which was used to increase the flight time differences between the various charge states.

Two microchannel plates (3 cm diameter) were mounted below the third stage in a chevron configuration and were followed by a resistive anode. The function of the resistive anode was to divide the deposited charge between the signal outputs, one of which was located at each of the four corners. The X and Y coordinates were related to the charge

signals by

$$X = \frac{C_1 + C_2}{C_1 + C_2 + C_3 + C_4} \quad \text{and} \quad Y = \frac{C_1 + C_4}{C_1 + C_2 + C_3 + C_4} ,$$

where C_1 is from the top right corner and the other charge signals are numbered clockwise. The position resolution, as determined with an ^{241}Am alpha particle source, was 1 mm. Several low transmission grids were mounted in front of the MCP to reduce the probability of detecting both ions from the same binary dissociation event.

A schematic diagram of the data acquisition system is shown in Fig. 2. Charge signals from the four corners of the resistive anode were sent through linear amplifiers to separate ADCs of a CAMAC interface. Fast timing signals were also taken from the resistive anode and used to start a TAC. The stop signals for the TAC were generated by beam particles striking another MCP positioned in the beam path directly behind the gas jet system (in place of the electron gun shown in Fig. 1). The output of the TAC was sent to a fifth ADC and the digitized data recorded event-by-event on magnetic tape via a MICROVAX computer system. Analysis of the data provides the positions and time-of-flight for each event.

An electron gun was constructed for use in characterizing the gas jet and testing the ion collection/time-of-flight spectrometer system. The design of the electron gun is also shown in Fig. 1. It consisted of a tungsten wire filament operated at a potential of -2500 V, an extractor electrode at -2400 V, a pair of collimators, and two sets of deflection plates which provided steering of the electron beam in both the x and y

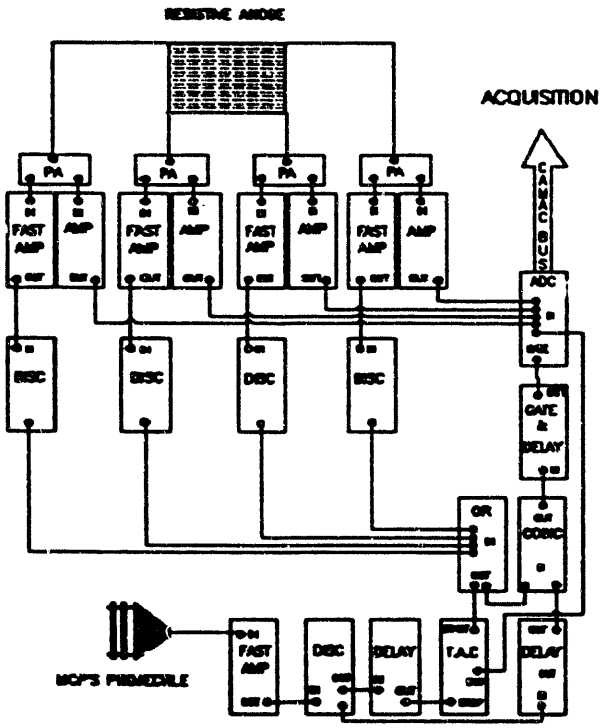

Figure 2. Schematic diagram of the data acquisition system.

directions. The electron gun generated a beam of electrons 1.5 mm in diameter of 1 μamp maximum intensity. The energy of the electron beam could be varied from a few hundred eV up to 2500 eV.

A profile of the gas jet in the region where it overlapped with the ion beam is shown by the position distribution obtained for N_2^{1+} molecular ions in Figure 3. These ions are produced with near-thermal energies since the recoil energy associated with single ionization is negligible [4]. The sharp structure in the main peak was caused by the grids in front of the MCP. This figure also shows the contribution from residual gas background along the beam path. The small peaks at both ends of the beam track are caused by focusing effects associated with nonuniformities in the electric fields near the periphery of the collection region.

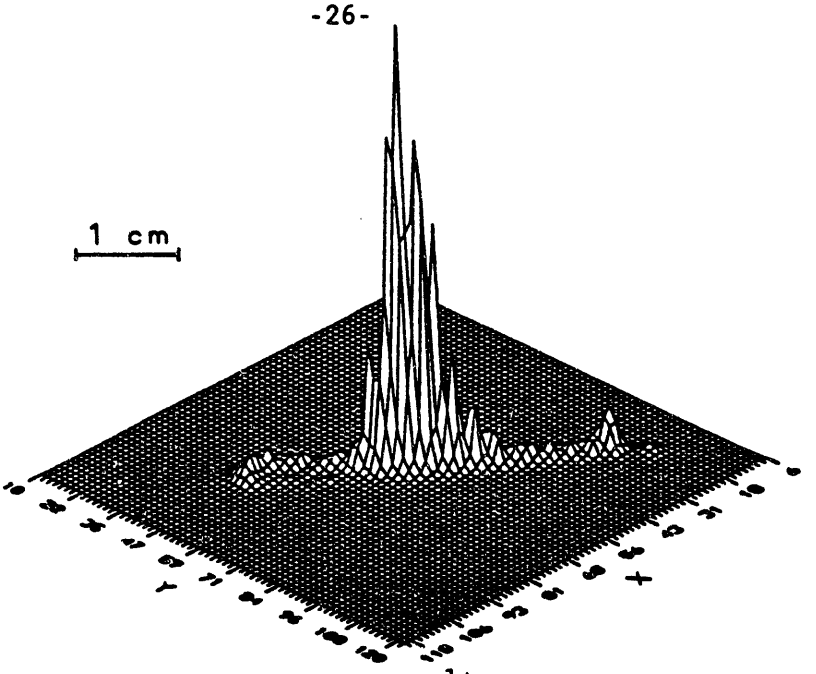

Figure 3. Position distribution of N_2^{1+} showing the profile of the gas jet where it overlapped the Ar beam.

The grid structure is shown more clearly in Figure 4(a) where the N_2^{1+} position distribution has been projected onto the X axis. The character of the background due to the residual gas is shown by the X projection of the position distribution of H_2O^{1+} in Figure 4(b).

The focusing effect encountered in the present experiments limited the analysis to N^{1+} and N^{2+} ions, for which the kinetic energy release was low enough that the peripheral region did not play a significant role. In order to assess the magnitude of any orientation effects, the position distributions were analyzed using a polar coordinate (R, θ) representation. The angles θ = 45 and 135 degrees were defined by the beam axis and R = 0 was defined by the intersections of the beam and gas jet axes. The method of analysis consisted of comparing the R and θ projections of the data with detailed simulations computed with different values of the asymmetry parameter α for an assumed angular dependence $d\sigma/d\Omega = k(1 + \alpha\sin\theta)$, where θ is the angle between the

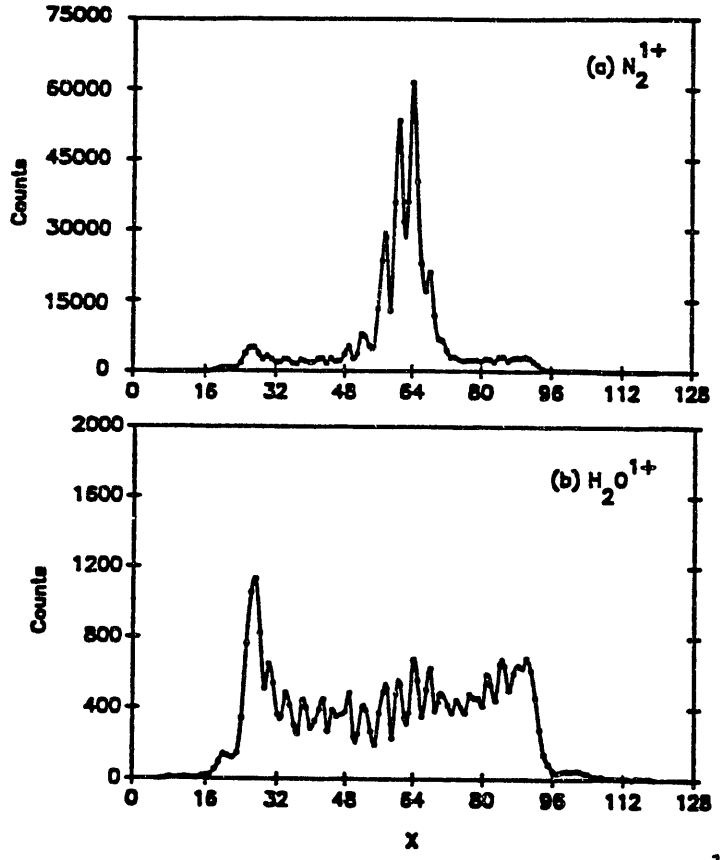

Figure 4. Projections onto the X axis of (a) the N_2^{1+} position distribution and (b) the H_2O^{1+} position distribution.

molecular axis and the ion beam axis. These simulations required the ability to calculate accurate trajectories of ions through the ion-collection/TOF spectrometer system, which in turn required a detailed knowledge of the electrostatic field profile, the jet density distribution over the interaction region, the kinetic energy of the ions of interest, and the background. The electrostatic field profile was generated using the electrostatic lens program SIMION [5]. The density distribution of the gas jet and the background were obtained from information provided by the position distributions for N_2^{1+}, H_2O^{1+}, and H^{1+}. The kinetic energy distributions were estimated from the results of previous measurements [6]. To test the method, detailed simulations

of the position distribution for isotropically emitted N_2^{1+} were performed. The experimental and simulated position distributions in R and θ coordinates are shown for N_2^{1+} in Figure 5. Although the R and θ units shown in this figure are arbitrary, the two angular positions at which the R distributions are the broadest correspond to the beam axis (i.e. θ = 45 and 135 degrees).

It was finally concluded that the sensitivity of the method is insufficient to detect asymmetries of $\alpha < 0.5$. In the present case of N^{2+}, coming primarily from the dissociation of N_2^{3+} molecular ions produced in direct ionization collisions, it was determined that $\alpha < 0.5$, and hence no evidence was found for an orientation dependence of the ionization cross section. Work is in progress on the development of an optical detection system that will enable reconstruction of the three-dimensional velocity distributions of both ions. If this effort proves successful, other more sensitive experiments will be performed to examine the orientation dependence of cross sections for transfer ionization.

References

[1] S. Cheng, C. L. Cocke, V. Frohne, E. Y. Kamber, and S. L. Varghese, Nucl. Instrum. Meth. B56, 78 (1991).

[2] K. Wohrer and R. L. Watson, Texas A&M Cyclotron Institute 1990-91 Progress Report, p. 54.

[3] J. A. Giordmaine and T. C. Wang, J. Appl. Phys. 31, 463 (1960).

[4] O. Heber, R. L. Watson, and G. Sampoll, Nucl. Instrum. Meth. B56, 232 (1991).

[5] D. A. Dahl and J. E. Delmore, Idaho National Engineering Laboratory report EGG-CD-7233 Rev. 1 (1987).

[6] G. Sampoll, R. L. Watson, O. Heber, V. Horvat, K. Wohrer, and M. Chabot, Phys. Rev. A45, 2903 (1992).

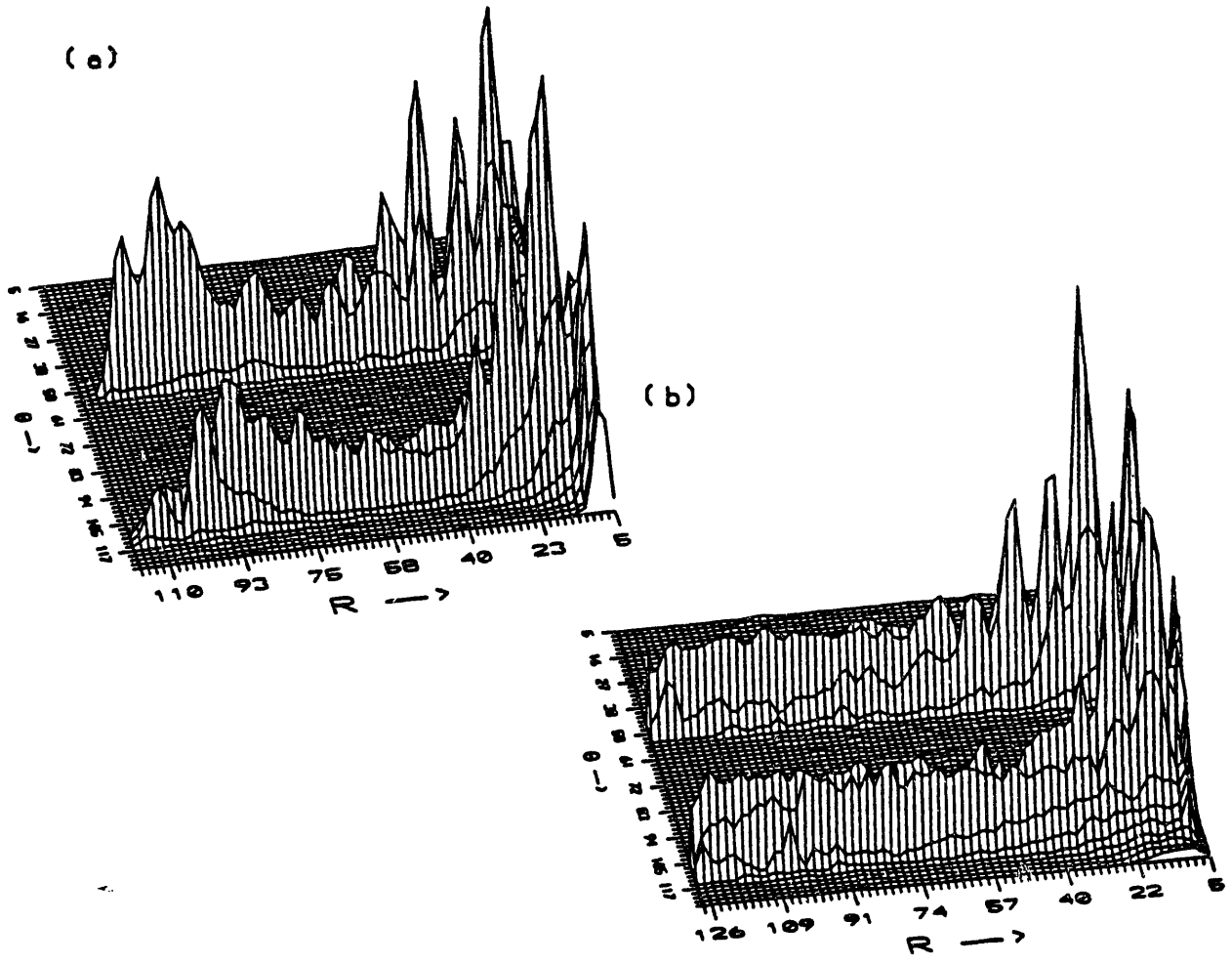

Figure 3. The (a) experimental and (b) simulated position distributions for N_2^{1+} plotted in R and θ coordinates.

D. Application of a Split-Anode Detector to Molecular Orientation Studies (V. Horvat, M. Chabot, and R. L. Watson)

An experiment to study the orientation dependence of the ionization of diatomic molecules in heavy-ion collisions by projecting the velocity distribution of the dissociation products onto a position sensitive MCP was described in the preceding article. Because this method did not yield satisfactory results, several other methods are under active consideration. The approach described here involves employment of a microchannel plate detector system having an anode composed of four segments that are insulated and shielded from each other. With such a system, it would be possible to measure the flight times of both fragment ions from a binary dissociation event and to identify the quadrant of the MCP into which each falls.

The orientation of the anode segments relative to the beam axis is shown in Fig. 1. In the binary dissociation of a diatomic molecule located along the symmetry axis, each fragment ion follows a trajectory which, under the influence of a uniform electric field, causes it to land in a quadrant of the MCP which is opposite to that of its partner. Therefore, the ratio $R = N_{AB}/N_{CD}$ provides the means for assessing the extent to which the angular dependence of ionization by heavy-ion impact deviates from isotropy. If the ionization cross section is independent of the angle between the internuclear axis and the beam axis, $d\sigma/d\Omega$ = constant (where $d\Omega = \sin\theta d\theta d\phi$), then it is obvious that $R = 1$ since the surface areas of a sphere through which the initial trajectories must pass to land in each quadrant of the MCP are equal. The distribution of

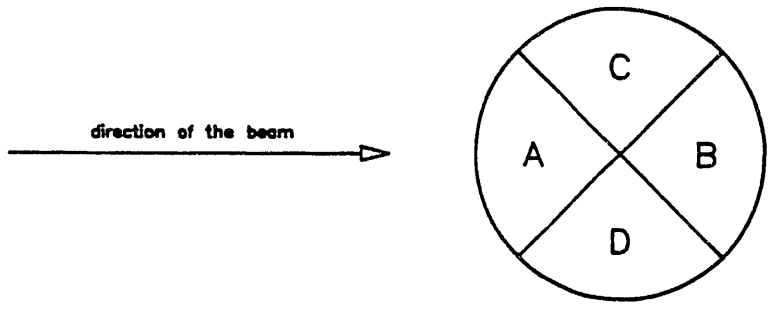

Figure 1. MCP detector anode as viewed from the center of the gas jet.

ion impact positions on the MCP for the case of isotropic ionization is shown in Fig. 2. This distribution was calculated for the dissociation $O^{2+} \longrightarrow O^{1+} + O^{1+}$ with a total kinetic energy release of 12 eV using a Monte Carlo procedure that took into account the theoretical shape of the gas jet.

If the ionization cross section displays a dependence on the angle α between the internuclear axis and the beam (i.e. an orientation dependence), then in general the ratio R will deviate from unity. Consider, for example, the following angular dependence which enhances the ionization cross section for parallel orientations of the internuclear axis relative to the beam axis:

$$d\sigma/d\Omega = a + b|\cos\alpha| \ , \qquad (1)$$

(The absolute value of $\cos\alpha$ is required by the fact that, for symmetric molecules, the differential cross section for $0 \leq \alpha \leq \pi/2$ must be the same as for $\pi/2 \leq \alpha \leq \pi$). The total cross section easily may be

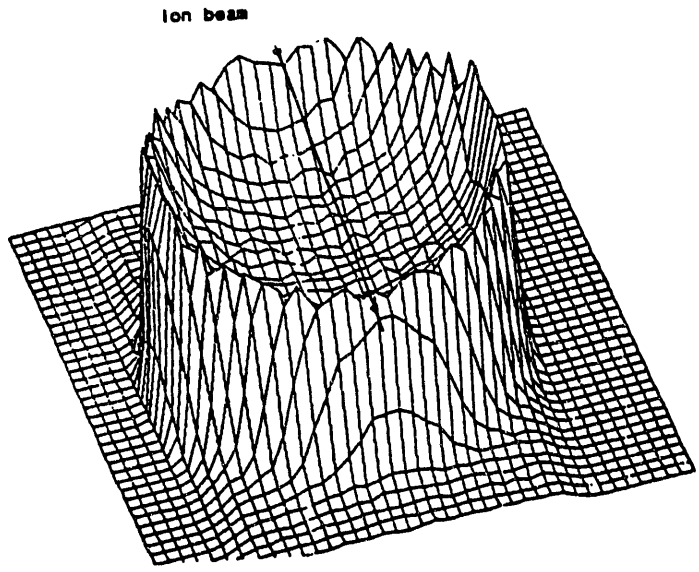

Figure 2. Simulation of the O^{1+} ion position distribution for isotropic dissociative ionization of O_2.

obtained by choosing the z-axis along the beam-axis (in which case $\alpha = \theta$) and performing the following integration:

$$\sigma_T = 2\int_0^{2\pi}\int_0^{\pi/2}(a + b\cos\theta)\sin\theta\, d\theta\, d\phi \ . \qquad (2)$$

The result is $\sigma_T = 2\pi(2a + b)$. The cross section for producing ions that will land in segments A and B of the MCP may be obtained by selecting the MCP symmetry axis as the z-axis (perpendicular to the beam axis) and noting that in this coordinate system, $\cos\alpha = \sin\theta\cos\phi$. Then,

$$\sigma_{AB} = 8\int_o^{\pi/4}\int_o^{\pi/2}(a\sin\theta + b\sin^2\theta\cos\phi)\, d\theta\, d\phi$$

$$= 2\pi(a + b\sqrt{2}/2) \ , \qquad (3)$$

and combining this with the above expression for the total cross section, the fraction of ions landing on segments A and B is obtained:

$$N_{AB}/N_T = \frac{(1 + \eta\sqrt{2}/2)}{(2 + \eta)} \quad , \tag{4}$$

where $\eta = b/a$. The cross section for producing ions that will land on segments C and D of the MCP may be worked out in a similar fashion. The fraction of ions that land on segments C and D is

$$N_{CD}/N_T = \frac{[1 + \eta(1 - \sqrt{2}/2)]}{(2 + \eta)} \quad . \tag{5}$$

The fractions N_{AB}/N_T and N_{AB}/N_{CD} calculated for a range of η values are given in Table 1.

A position distribution was calculated for the dissociative ionization $O_2 \longrightarrow O_2^{2+} \longrightarrow O^{1+} + O^{1+}$ (total kinetic energy release of 12 eV) assuming a differential cross section of the form $1 + \sin\alpha$ (i.e. enhanced ionization for perpendicular orientations, with $\eta = 1$. This distribution is shown in Fig. 3.

Table 1. Fractions of ions landing on segments AB and CD calculated as a function of η.

η	N_{AB}/N_T (%)	N_{AB}/N_{CD}
0	50.0	1.00
0.25	52.3	1.10
0.50	54.1	1.18
1.00	56.9	1.32
∞	70.7	2.41

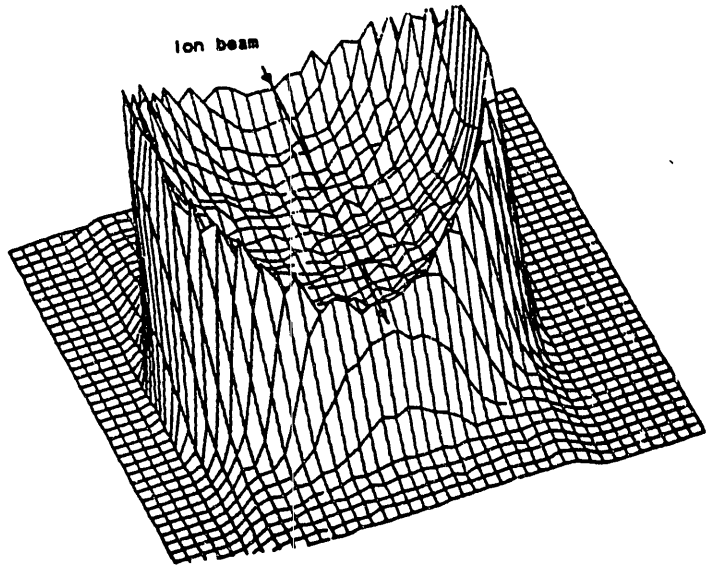

Figure 3. Simulation of the O^{1+} ion position distribution for an angular dependence $d\sigma/d\Omega = 1 + \sin\alpha$.

E. Experiments with the Texas A&M ECR Ion Source

(R. L. Watson, T. Lotze, B. B. Bandong, M. Chabot, and O. Heber)

The recent construction of an electron-cyclotron-resonance (ECR) ion source has greatly extended the research capabilities of the Texas A&M K500 superconducting cyclotron and, in addition, has provided access to experimentation with beams of low-energy, highly-charged ions. The ability to use ionic charge as an experimentally variable parameter in a velocity regime in which the total potential energy of the ion dominates over its kinetic energy provides a powerful probe for the investigation of multielectron charge transfer and neutralization processes. Moreover, the availability of such beams provides unique opportunities to significantly advance the fundamental understanding of slow ion-atom collisions and to explore applications to materials characterization and modification. This report briefly describes the characteristics of the ECR source, the atomic physics beamline attached to the source, and two experiments currently in progress.

The Texas A&M ECR ion source source is medium-sized with a Sm-Co hexapole surrounding the 13.7 cm diameter second stage. Microwave power for the source is provided by a 2.0 KW, 14.5 GHz transmitter for the first stage and a 3.25 KW, 6.4 GHz transmitter for the second stage. The source gas is injected on axis through a small orifice at the left end of the first stage. Plasma produced in the first stage exits through a collimator at the right end and travels through a hole in the gas baffle into the second stage. Ions are extracted from the second stage with energies up to 13 keV/charge by means of an electrostatic

lens. A more detailed description of the ECR source is given in Ref. [1]. Representative ion intensities for an extraction voltage of 10 kV are listed in Table 1.

Table 1. Representative ion currents (eμA) from the TAMU ECR ion source with an extraction voltage of 10 kV.

Ion	Current
$^{14}N^{5+}$	45
$^{16}O^{5+}$	60
$^{16}O^{6+}$	60
$^{16}O^{7+}$	8
$^{40}Ar^{8+}$	30
$^{40}Ar^{9+}$	27
$^{40}Ar^{11+}$	14
$^{40}Ar^{13+}$	3
$^{84}Kr^{19+}$	2

A schematic diagram of the the atomic physics beamline, which recently has been built to accommodate experiments with ECR source beams, is shown in Fig. 1. The beamline is constructed from sections of Ni-electroplated, low-carbon steel pipe to help shield against the magnetic field from the cyclotron. The primary focusing elements for the atomic physics beamline are two electrostatic asymmetric quadrupole triplets. The first triplet focuses the beam through a pipe segment (labeled "beam steering and diagnostics" in Fig. 1) which contains adjustable horizontal and vertical slits, a pair of deflection plates, a

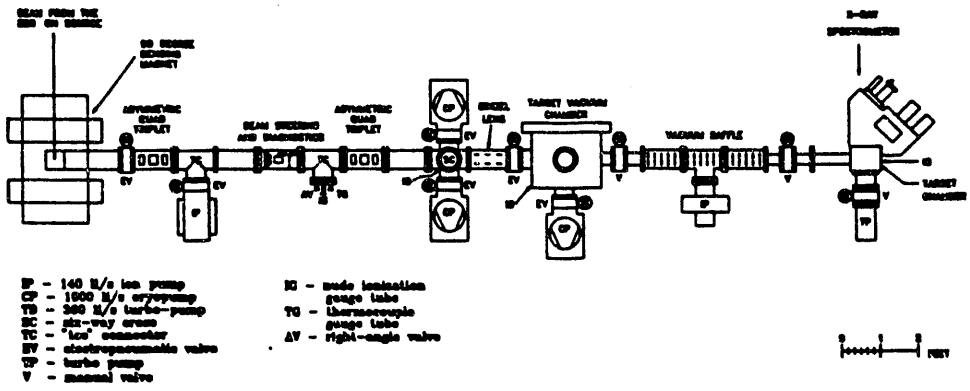

Figure 1. Schematic diagram of the atomic physics beamline on the ECR ion source.

rotatable wire beam profile monitor, and a Faraday cup. The second quadrupole triplet focuses the beam through a 6-way cross into a 41 cm diameter scattering chamber. An Einzel lens is located between the 6-way cross and the scattering chamber.

The 6-way cross provides additional experimental flexibility in that it can be used as another target chamber. A 10^3 l/s cryopump is attached to one arm and the cross itself can be isolated from the upstream and/or downstream segments of the beamline by means of two pneumatic valves. A differentially pumped charge exchange cell can be inserted into the 6-way cross. The charge exchange cell consists of a metal cylinder closed on one end and attached to a 10^3 l/s cryopump on the other end. The cylinder contains 1.25 cm entrance and exit apertures for the beam to pass through. When it is in use, another set of 1.25 cm entrance and exit apertures are placed in the upstream and downstream arms of the 6-way cross to collimate the beam and to limit gas flow to the beamline and scattering chamber.

The portion of the atomic physics beamline in front of the 6-way cross is evacuated by a 400 l/s ion pump, which attains a base pressure

of 1.8×10^{-8} without baking. Both the 6-way cross and the scattering chamber are evacuated by separate 10^3 l/s cryopumps, which maintain the scattering chamber at a base pressure of 1×10^{-8} without baking. All components of the atomic physics beamline are ultrahigh vacuum compatible. A vacuum baffle consisting of a 48 cm long, 11 cm diameter tee containing a series of 18 apertures of 2.5-cm diameter in the straight-through section and a 50 l/s ion pump connected to the perpendicular arm is attached to the exit port of the scattering chamber. This device enables experiments to be performed behind the scattering chamber at pressures as high as 10^{-6} Torr without significantly degrading the scattering chamber vacuum. A small target chamber and a curved crystal x-ray spectrometer are currently mounted at the end of the beamline.

The ion optics (including the bending magnets and solenoids in front of the atomic physics beamline) transport approximately 40% of the extracted, charge-to-mass analyzed beam from the ECR source to the scattering chamber. With the charge exchange cell and its apertures installed, the amount of beam transported to the scattering chamber drops to approximately 10%, but in this case the focused spot size is less than 5 mm in diameter.

One of the experiments, currently in progress, that utilizes beams from the ECR ion source involves high resolution measurements of oxygen x-rays emitted during the neutralization of O^{7+} ions slowing down and stopping in a gold target. As a slow, highly charged ion approaches a metal surface, electrons begin transferring from the surface to the ion at distances of the order of Qe^2/Φ, where Q is the ion charge and Φ is

the work function of the solid. Neutralization of the ion is expected to proceed via a series of resonant capture and Auger de-excitations [2,3].

A number of recent experiments have shown that level crossing mechanisms exist for producing inner-shell vacancies in both projectile ions and surface atoms during the neutralization interaction [4]. The time scale for neutralization is an important parameter for characterizing the mechanisms involved. Very slow ions incident on metal surfaces may be totally neutralized before they enter the surface. The local charge depletion is then spread to the bulk on a time scale comparable to the plasma frequency. A recent experiment performed elsewhere has demonstrated the possibility of using high resolution x-ray spectroscopy to delineate the time scale for filling K- and L-vacancies in so called "hollow atoms" formed as a result of the capture of electrons to Rydberg states during the neutralization process [5].

The high resolution x-ray measurements currently in progress here employ a curved crystal spectrometer and are designed to take advantage of the high reflectivity and good resolution properties of thallium acid phthalate (TAP) crystals for oxygen x-rays, which should make it possible to clearly resolve the $K\alpha$ satellite and hypersatellite groups associated with different numbers of L-vacancies. Thus far, the target chamber and spectrometer system have been adapted to the atomic physics beamline and tested with an electron gun. In a recent run with 91 keV O^{7+} ions, 1.8 μamp of beam was extracted from the ECR ion source, but only 10 namp of beam was obtainable on the target. This beam current was sufficient to accumulate the pulse height spectrum of oxygen K x-rays shown in Fig. 2,

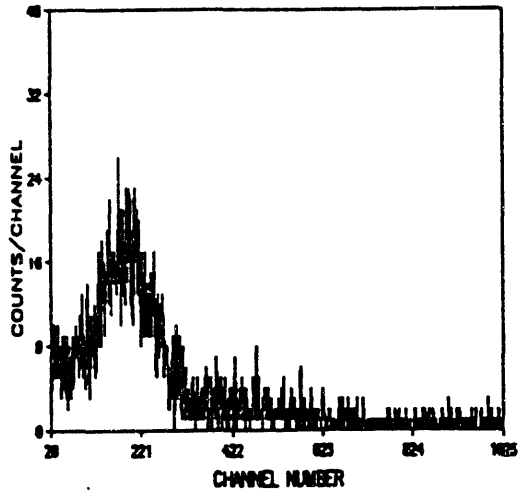

Figure 2. Pulse height spectrum of oxygen K x-rays from 70 keV O^{7+} stopping in a gold surface. The x-rays were reflected from a TAP crystal at the highest intensity angle and detected in a thin-window flow proportional counter.

but was much too low to make the desired high resolution measurements. Further progress on this project will require improvement of the beam transport and focusing elements along the atomic physics beam line.

Measurements of charge state distributions produced in low energy charge exchange collisions employing time-of-flight (TOF) spectroscopy are in preparation. A TOF spectrometer and gas cell have been constructed to fit in place of the charge exchange cell in the 6-way cross. A diagram of the system, showing the equipotential lines and the trajectories of 70 keV O^{7+} ions calculated using the electrostatic lens program SIMION [6] is presented in Fig. 3. Ions produced in the target gas by charge exchange collisions are accelerated out of the cell by a uniform electric field into a 12 cm flight tube. At the end of the flight tube, they are further accelerated into a chevron microchannel plate detector system. The projectile ions are deflected by the electric field and exit through a slit in the gas cell. They are then detected by means of a position sensitive microchannel plate which

provides charge state identification and stop signals for the time-to amplitude converter used to measure the target-ion flight times.

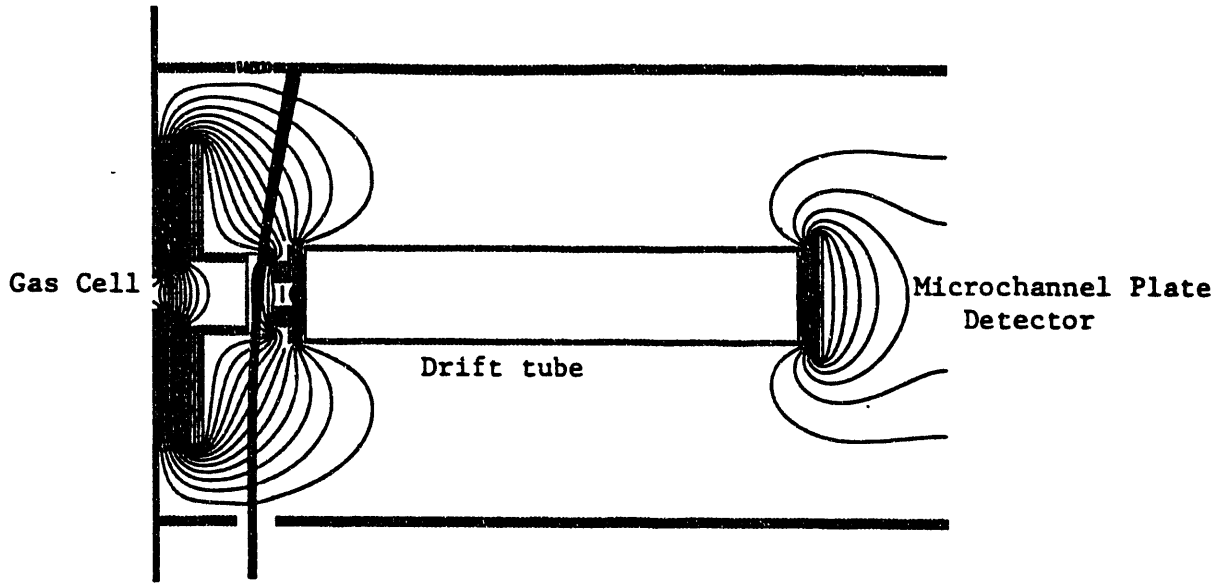

Figure 3. Diagram of the gas cell and TOF spectrometer for the charge exchange measurements.

References

[1] D. P. May, R. C. Rogers, P. Smelser, G. Mouchaty, A. van Baalen, and P. Bowman, Proceedings of the International Conference on ECR Ion Sources and their Applications, East Lansing, MI (Edited by J. Parker), NSCL Report MSUCP-47 (1987) 364.

[2] H. D. Hagstrum and G. E. Becker, Phys. Rev. 88 (1973) 107.

[3] F. W. Meyer, C. C. Havener, S. H. Overbury, K. J. Reed, K. J. Snowdon, and D. M. Zehner, J. Physique 50 (1989) C1-263.

[4] C. C. Havener, K. J. Reed, K. J. Snowdon, N. Stohlterfoht, D. M. Zehner, and F. W. Meyer, Surf. Sci. 216 (1989) L357.

[5] J. P. Briand, L. de Billy, P. Charles, S. Essabaa, P. Briand, R. Geller, J. P. Desclaux, S. Bliman, and C. Ristori, Phys. Rev. Lett. 65 (1990) 159.

[6] D. A. Dahl and J. E. Delmore, Idaho National Engineering Laboratory report EGG-CD-7233 Rev. 1 (1987).

F. Ionization of Noble Gas Atoms by Alpha Particles and Fission Fragments from the Decay of ^{252}Cf

(B. M. Hill, R. L. Watson, K. Wohrer, B. B. Bandong, G. Sampoll, and V. Horvat)

The ionizing properties of fission fragments passing through matter have been of continuing interest since the discovery of nuclear fission over half a century ago. In recent years, the development of ^{252}Cf plasma desorption mass spectrometry (PDMS) [1] has refocused attention on various aspects of this topic. While the energy loss and charge equilibration properties of MeV heavy ions in general have been fairly well characterized experimentally, many details of the ionization process still remain to be elaborated. An unresolved issue relating to the PDMS technique concerns the nature of the mechanism for desorbing large molecules from surfaces without inducing sufficient internal excitation to cause fragmentation. Of fundamental importance to a complete understanding of this process is a detailed knowledge of the ionization mechanisms and cross sections for single ion-atom collisions.

The primary objective of the present investigation was to determine the cross sections for the ionization of free atoms in single collisions with alpha particles and fission fragments from the decay of ^{252}Cf as a function of the number of electrons removed. An additional objective was to evaluate ^{252}Cf as a source of energetic heavy ions for use in studies of multielectron ionization of atoms and molecules in the gas phase.

The radionuclide ^{252}Cf decays by alpha particle emission (96.9%)

and spontaneous fission (3.1%) with a half life of 2.638 years [2]. The principal alpha decay branch (84.0%) is to the ground state of ^{248}Cm with an alpha energy of 6.118 MeV. The most probable (post neutron emission) fission fragments formed in the spontaneous fission of ^{252}Cf are ^{142}Cs and ^{106}Tc, having average kinetic energies of 79 and 104 MeV, respectively [3,4]. The average equilibrium ionic charge of a fission fragment, estimated using the semi-empirical formula of Shima et al. [5] is 20+.

A diagram of the differentially pumped gas cell system employed in the present measurements is shown in Fig. 1. A small chamber housing a gas cell and a time-of-flight (TOF) spectrometer was mounted inside a 30 cm diameter stainless steel vacuum chamber. A 2400 L/s diffusion pump attached to the bottom of the main chamber pumped directly on the gas cell chamber, while a 1200 L/s diffusion pump maintained the vacuum at an acceptable level in the main chamber. The gas cell consisted of a Cu tube 1.8 cm long and 1.7 cm in diameter surrounded by a nylon holder.

A ^{252}Cf source was mounted on the side of the nylon holder. Fission fragments and alpha particles from the source entered the cell through a 3 mm diameter hole in the Cu tube and those particles that passed through a 4 mm diameter hole located directly across the cell from the source ($\approx$ 78 fission fragments/s and 1400 alpha particles/s) were detected by a Si surface barrier detector (SBD) mounted in the nylon holder on the opposite side. The hole in front of the detector was covered with an 88% transmission Ni grid to minimize the influence of stray electric fields on the ions produced inside the cell. The ^{252}Cf source consisted of a 4 mm diameter spot of Cf_2O_3 electroplated

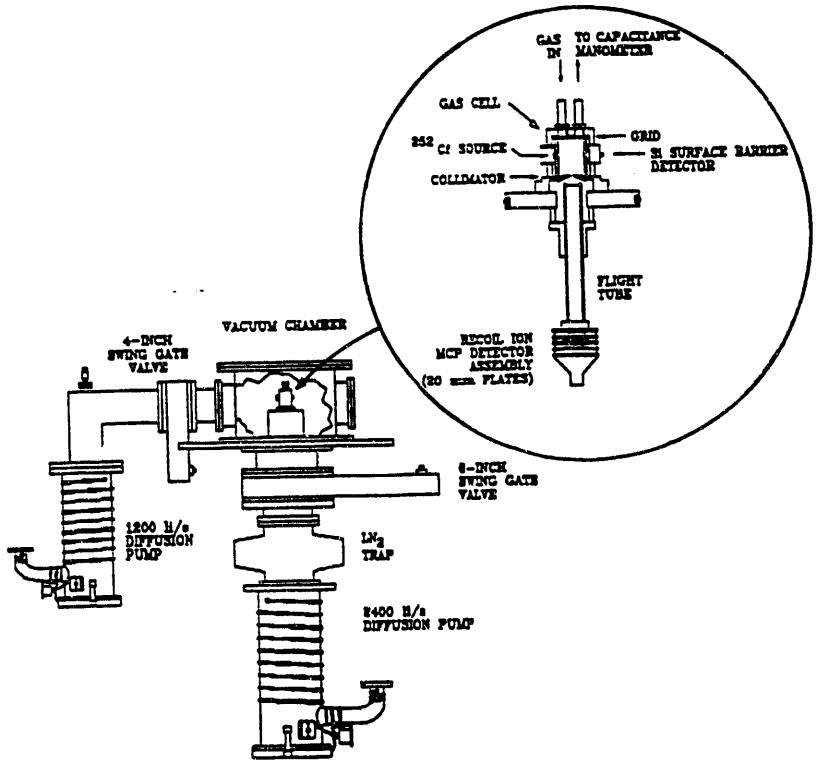

Figure 1. Schematic diagram of the experimental apparatus.

onto a 50 $\mu g/cm^2$ layer of Au on a 1 mg/cm^2 Ni backing foil and covered with another Au/Ni foil of identical construction [6]. The fission fragments and alpha particles lost approximately 30 MeV and 0.5 MeV, respectively, in passing through the Au/Ni foil.

A brass collimator ring (2.7 mm hole diameter), positioned at the bottom of the gas cell and electrically insulated from the Cu cylinder, restricted the flow of gas out of the cell. Gas entered the cell through an inlet tube at the top of the nylon holder and its pressure was regulated by means of a capacitance manometer and an external needle valve. During the experimental measurements, the pressure in the gas

cell was nominally kept at 1 mTorr while the pressure in the main chamber was in the low 10^{-5} Torr range.

An electric field was created inside the gas cell by placing 1250 V on the top grid and 400 V on the collimator ring (see the inset in Fig. 1). The grounded entrance grid of the flight tube was positioned 2 mm below the gas cell collimator ring. At the other end of the 12.5 cm flight tube, a set of microchannel plates (MCP) in a chevron configuration served as the ion detector. Ions produced by fission fragment or alpha particle collisions were accelerated toward the collimator by the electric field in the gas cell. Those ions that made it through the collimator opening were further accelerated by the electric field between the collimator ring and the entrance grid to the TOF spectrometer. The time resolution of the TOF spectrometer was optimized by varying the voltage on the collimator ring until the best space focus [7] was achieved.

Fast timing signals from the SBD preamplifier were sent through a fast filter amplifier to a constant fraction discriminator (CFD). The output of the CFD provided the start signals for a time-to-amplitude converter (TAC). Signals from the MCP were sent through a fast amplifier to another CFD and the output of this CFD provided the stop signals for the TAC. The output signals from the TAC went to a CAMAC analog-to-digital converter (ADC1) interfaced to an IBM-compatible 486 personal computer. Energy signals from the SBD preamplifier were routed through a linear amplifier to another CAMAC ADC (ADC2). Gate signals for the ADC's were generated by the TAC output and the two parameters recoil-ion TOF and projectile energy were recorded on disk event-by-

event for every valid TAC signal.

The TOF spectra for alpha particle and fission fragment projectiles were separated off-line by sorting the data with respect to projectile energy. A narrow window was used to select the alpha particle energy peak and a very wide window was required to include the broad energy distribution for fission fragments. The resulting TOF spectra obtained for an Ar target are shown in Fig. 2. The alpha particle spectrum (Fig. 2a) displays clearly discernible peaks for Ar ions having charges of 1+ to 6+. The immense increase in ionizing power in going from alpha particles to fission fragments is evident in Fig. 2b, where TOF peaks for Ar ions ranging in charge from 1+ to 13+ are visible. Several other small peaks due to N_2, O_2, and H_2O impurities in the gas cell also appear in these spectra.

The time resolution for the Ar^{1+} peak was about 8 ns (full width at half maximum) and was determined primarily by the size of the projectile beam, which limited the effectiveness of the space focusing. The recoil-ion kinetic energies also contributed substantially to the widths of the peaks for the higher charge states [8].

Large tails (especially noticeable for Ar^{1+}) appear on the right sides of the TOF peaks in Fig. 2. These tails were partly caused by charge-changing collisions between recoil-ions and target atoms during the acceleration stage. However, a study of the Ar^{1+} peak shape as a function of gas pressure revealed that a substantial portion of the tail was independent of the gas density and hence must have been caused by the projectile beam size or some other (unknown) mechanism.

A TOF spectrum obtained for fission fragment collisions with Xe

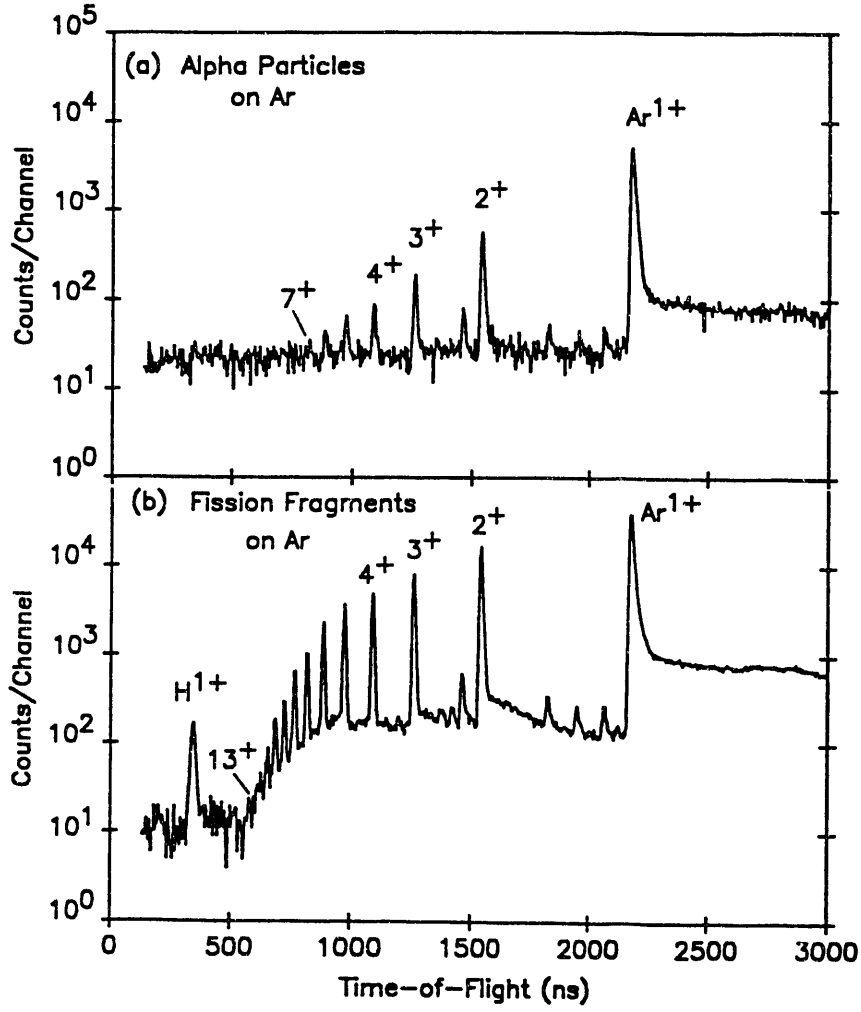

Figure 2. Time-of-flight spectrum of Ar recoil-ions produced in (a) alpha particle and (b) fission fragment collisions.

atoms is shown in Fig. 3. Although the highest charge states are not resolvable in this spectrum, it is estimated from a calibration of $Q^{-1/2}$ versus TOF performed for the resolved charge states, that the maximum recoil-ion charge produced in this collision system is approximately 20+. The total ionization energy required to remove this many electrons is 4750 eV [9]. The maximum charge states produced in the various

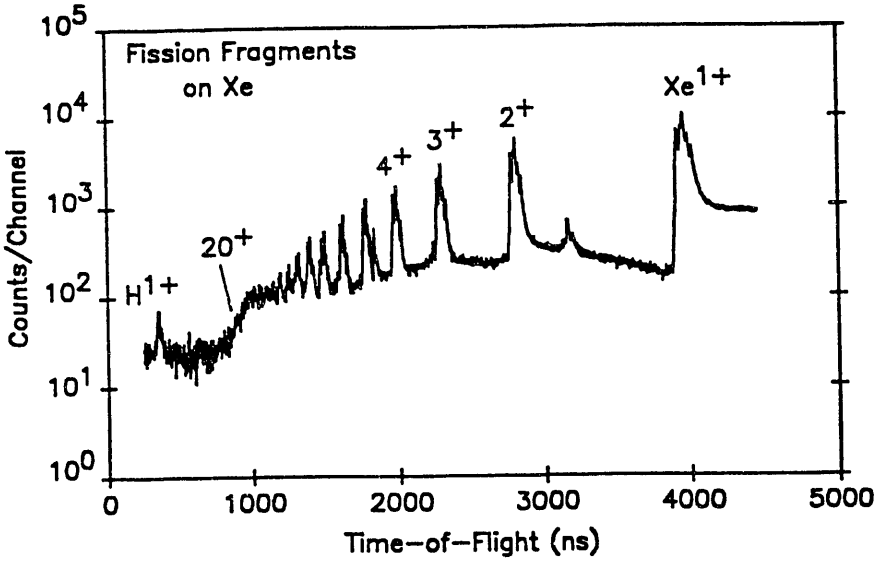

Figure 3. Time-of-flight spectrum of Xe recoil-ions produced in fission fragment collisions.

targets by alpha particle and fission fragment collisions are listed in Table 1 along with the corresponding total ionization energies.

A slight enhancement of the production yields for the higher charge states of Xe (around Q = 15+) is evident in Fig. 3. This behavior, which was also observed in the spectrum obtained for Kr around Q = 11+, indicates that these yields contain appreciable contributions from collisions in which the projectile captured one or more electrons [10].

The measured recoil-ion yields N_n are related to their respective n-fold ionization cross sections σ_n by the following formula:

$$N_n = N_p \sigma_n \rho \ell T \xi \ , \qquad (1)$$

where N_p is the number of projectiles, ρ is the number density of target

atoms (i.e. atoms/cm^3), ℓ is the effective target length (cm), T is the transmission probability through the TOF spectrometer, and ξ is the detection efficiency of the MCP. Large uncertainties were associated with several of the above quantities. The manometer used to measure the gas pressure was connected to the gas cell by means of a 15 cm length tube of 6.4 mm diameter. The unknown pressure differential between the cell and the manometer was a potential source of error in the determination of the target atom density. Although the transmission probability through the TOF spectrometer could be calculated with fair reliability, the MCP efficiency could not be directly measured. The detection efficiency is expected to roughly correspond to the open-channel area fraction (0.55 in the present case), but measured efficiencies for keV ions have been found to range from 0.3 to 0.8 [11].

Table 1. Maximum recoil-ion charge states and their corresponding total ionization energies (in eV).

Projectile:	Alpha Particles		Fission Fragments	
	Q_{max}	E_T	Q_{max}	E_T
Target:				
He	2	79	2	79
Ne	5	349	8	954
Ar	6	309	12	2635
Kr	6	271	15	3090
Xe	6	244	20	4750

Because of the uncertainties described above, the recoil-ion production cross sections deduced from the present measurements were normalized to the theoretical cross section (8.55×10^{-17} cm^2) calculated for He^{1+} production by 5.8 MeV alpha particles using the ECPSSR formulation [12]. Measured K-shell ionization cross sections for low-Z projectiles have been shown to be very well reproduced by this model [13]. It was reassuring to find that the He^{1+} cross section obtained from the measured yield using the best estimates of the target atom density and MCP efficiency was in excellent agreement with the theoretical cross section.

The recoil-ion production cross sections are presented in Fig. 4. The alpha particle cross sections decrease rapidly with increasing number of electrons removed. Moreover, the cross sections for the removal of more than one electron ($n > 1$) are quite sensitive to the target atomic number (Z_2) and roughly increase as $Z_2^{1.8}$. In comparison, the fission fragment cross sections are larger by about a factor of 25, they display a much slower rate of decrease with increasing n and they exhibit very little dependence on target atomic number. In fact, the fission fragment cross sections cluster together in two sets; one for the He and Ne targets and one for the Ar, Kr, and Xe targets. The same grouping also occurs for the $n = 1$ alpha particle cross sections. This clustering effect of the cross sections is probably a direct consequence of the outer-shell electron binding energies. Shown in Fig. 5 are the total ionization energies for the consecutive removal of outer-shell electrons from the target atoms in question [9,14]. It is evident that the ionization energies are grouped together in the same manner as the fission fragment ionization cross sections.

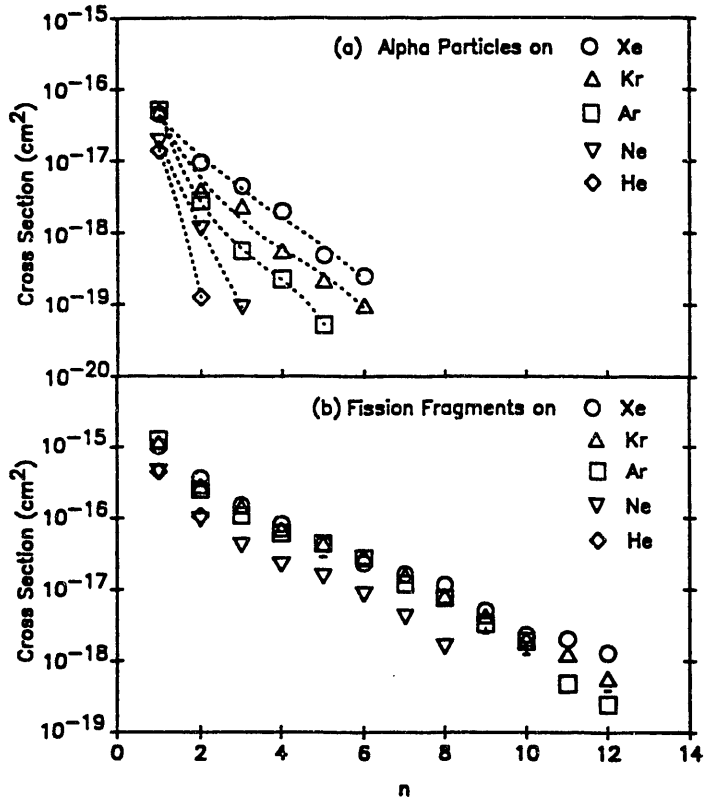

Figure 4. Cross sections for recoil-ion production in (a) alpha particle collisions and (b) fission fragment collisions as a function of the number of electrons removed.

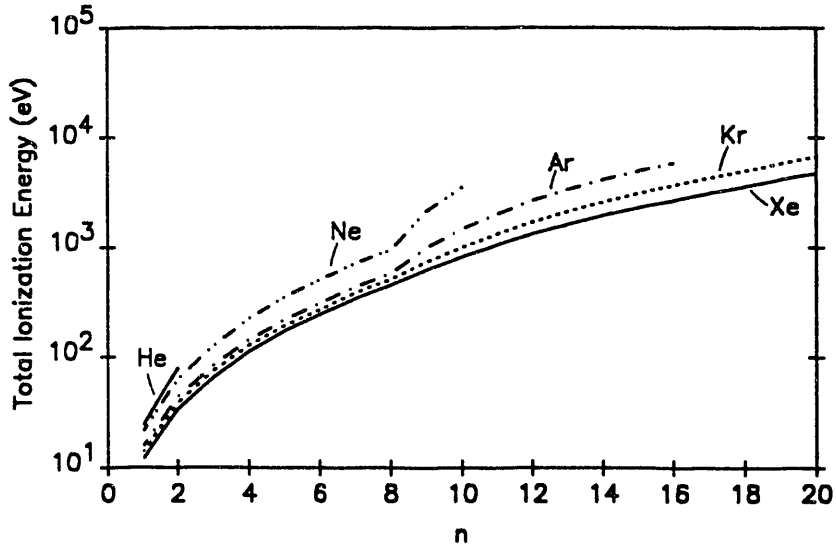

Figure 5. Total ionization energies for the removal of n electrons.

In numerous studies of recoil-ion production by 0.5 to 2 MeV/amu heavy ions from particle accelerators [15], it has been found that the cross sections for multiple ionization are well represented by a simple independent electron approximation [16]. Within the framework of this model, the cross section for the removal of n electrons is calculated using the expression

$$\sigma_n = 2\pi \int_0^\infty bP_n(b)db \ , \qquad (2)$$

where b is the impact parameter and $P_n(b)$ is the total probability of removing n electrons from a shell containing N electrons, given by

$$P_n(b) = [{}^N_n]p(b)^n[1 - p(b)]^{N-n} \ . \qquad (3)$$

In the above formula, $[{}^N_n]$ is a binomial coefficient and p(b) is the single-electron ionization probability. A simple analytical function that is commonly employed to represent p(b) [17] is

$$p(b) = p_o\exp(-b/r_s) \ , \qquad (4)$$

where p_o is the single-electron ionization probability at b = 0 and r_s is a radius parameter.

The model described above has been applied to the present cross section data for Xe in order to provide an estimate of the distances involved in multiply ionizing collisions of fission fragments. Only the outermost shell of 8 electrons was considered in these calculations. The experimental cross sections for n = 1 and n = 3 were used to establish the optimum values of p_o (0.57 for alpha particles and 0.95

for fission fragments) and r_s ($0.84a_o$ for alpha particles and $3.7a_o$ for fission fragments. The results are shown in Fig. 6 where it may be seen that the calculated cross sections for the other values of n, up to n = 7 in the case of fission fragments, are in good agreement with the experimental cross sections. The model underestimated the fission fragment cross section for n = 8 by 65%. This fact provides additional evidence that electron capture collisions, which are characterized by different p_o and r_s values, play an important role in the production of the high charge states.

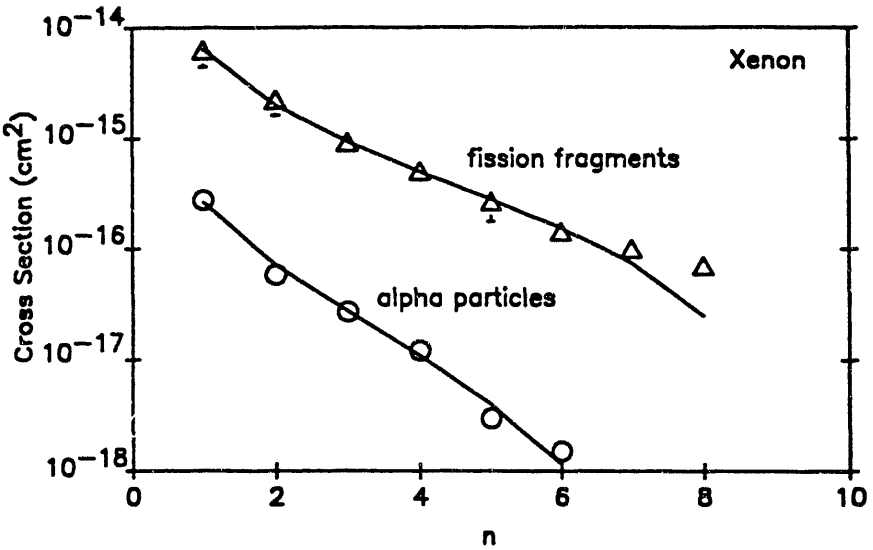

Figure 6. Comparison of the experimental cross sections for Xe recoil-ion production in alpha particle and fission fragment collisions (data points) with those predicted by the independent electron model calculations (solid lines).

REFERENCES

[1] D. F. Torgerson, R. P. Skowronski, and R. D. Macfarlane, Biophys. Res. Commun. 60 (1974) 616.

[2] Table of Isotopes, 7th edition, Edited by C. M. Lederer and V. Shirley (John Wiley & Sons, New York, 1978).

[3] H. W. Schmitt, W. E. Kiker, and C. W. Williams, Phys. Rev. 137 (1965) B837.

[4] R. L. Watson, Ph.D. dissertation, University of California Lawrence Radiation Laboratory Report UCRL-16798 (1966).

[5] K. Shima, T. Ishihara, and T. Mikumo, Nucl. Instr. and Meth. 200 (1982) 605.

[6] Source supplied by Isotope Products Laboratories, 1800 N. Keystone St., Burbank, California 91504 USA.

[7] W. C. Wiley and I. H. McLaren, Rev. Sci. Instr. 26 (1955) 1150.

[8] O. Heber, R. L. Watson, and G. Sampoll, Nucl. Instr. and Meth. B56 (1991) 232.

[9] T. A. Carlson, C. W. Nestor, Jr., N. Wasserman, and J. D. McDowell, Atomic Data 2 (1970) 63.

[10] T. J. Gray, C. L. Cocke, and E. Justiniano, Phys. Rev. A22 (1980) 849.

[11] Channelplate Charged Particle Detectors, (unpublished report by Comstock Incorporated, P.O. Box 199, Oak Ridge, Tennessee, 37830, USA).

[12] G. Lapicki and F. D. McDaniel, Phys. Rev. A23 (1981) 975.

[13] G. Lapicki, J. Phys. Chem. Ref. 18 (1989) 111.

[14] C. E. Moore, Atomic Energy Levels, NSRDS-NBS 35 (1971), U.S. Government Printing Office, Washington, D.C. 20402.

[15] See for example A. Muller, B. Schuch, W. Groh, and E. Salzborn, Z. Phys. D7 (1987) 251, and references therein.

[16] J. H. McGuire and L. Weaver, Phys. Rev. A16 (1977) 41.

[17] P. H. Mokler and H. D. Lissen, in Progress in Atomic Spectroscopy, edited by H. F. Berger and H. Kleinpoppen (Plenum, New York, 1983), p. 321.

G. Auger Electron Spectrum of 8 MeV/amu Ar^{7+}

(V. Horvat, R. Paramaswaran, G. Sampoll, R. L. Watson, M. Barrett, B. Griffith, R. D. DuBois#, L. H. Toburen#, and D. Schneider*)

A parallel-plate, tandem-type, zero-degree electron spectrometer, together with a collision chamber (including two sets of four-jaw adjustable slits and a 1500 L/s turbomolecular pumping system), on loan from Lawrence Livermore National Laboratory, is being used to study the spectra of electrons resulting from the interaction of high-energy multiply-charged ion beams from the K-500 cyclotron with gas and solid targets. A schematic diagram of the system is shown in Figure 1. A channeltron has been adapted to the spectrometer to serve as the electron detector. A Faraday cup with a biased electron-suppresser ring provides normalization of the counting intervals during the spectrometer voltage scans. The gas cell is attached to a gas supply and control system that includes an automatic valve and a capacitance manometer. Precise alignment of the spectrometer, the gas cell, and the slits is achieved visually by means of a transit.

Operation of the spectrometer is controlled by a PC-based control and data acquisition system, described in the next report. A simple electron gun was constructed to test the electron spectrometer system and to accurately calibrate the energy scale. In the calibration procedure, the voltages on the spectrometer and the electron gun were measured using a four-digit precision digital voltmeter. The spectrometer was tested both in the low resolution (high transmission)

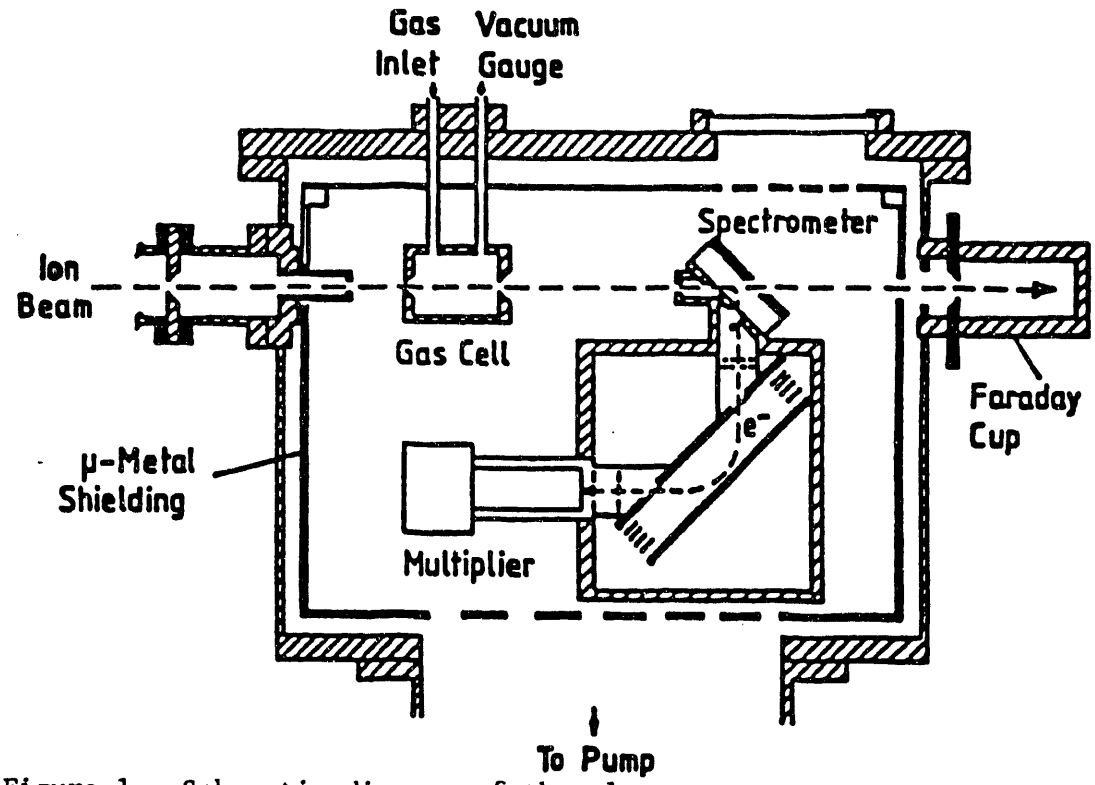

Figure 1. Schematic diagram of the electron spectrometer system (taken from Ref. [1]).

mode and in the high resolution (low transmission) mode. A typical spectrum of electrons from the electron gun measured in the high resolution mode is shown if Figure 2. With 2 mm slits at the entrance and exit of the second stage of the electron spectrometer, the energy resolution was found to be 2.4% in the low resolution mode, and 2.4% of the pass energy in the high resolution mode.

The performance of the electron spectrometer system was tested in preliminary measurements of electrons from 8.05 MeV/amu Ar^{7+} projectiles interacting with an Ar gas target at a pressure of 40 mTorr. The spectrum of Auger electrons emitted from projectiles in the backward (180^{o}) direction was recorded. The beam energy was accurately determined from the cusp electron spectrum and used to transform the Auger spectrum to the projectile rest frame. The resulting spectrum is

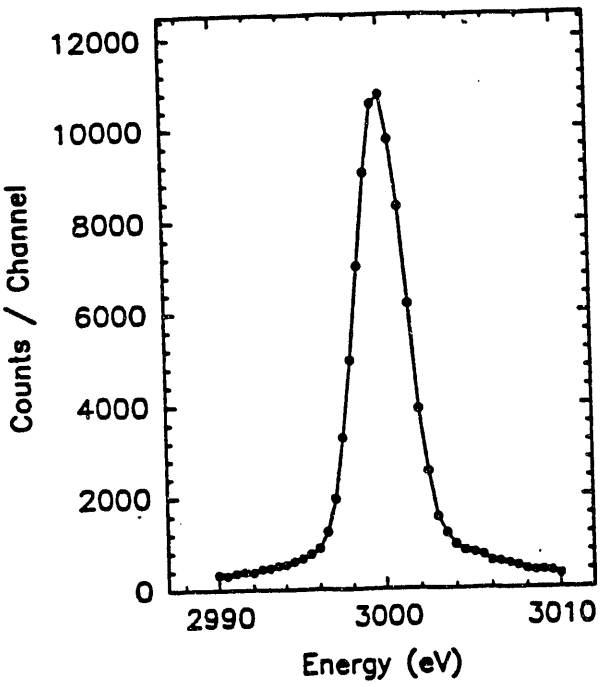

Figure 2. Spectrum of electrons from the electron gun measured in high resolution mode with a pass energy of 100 eV.

shown in Figure 3. Four groups of peaks, labeled A, B, C, and D, are observable in this spectrum. To identify the transitions responsible for these peaks, the multiconfiguration Dirac-Fock program of Desclaux [2] was employed to calculate the transition energies between the possible initial and final state configurations. Since the projectile electron configuration prior to the interaction with the target is predominantly $1s^2 2s^2 2p^6 3s$, L-Auger electrons from the projectile can be emitted only via the excitation of one (or more) of the L-shell electrons into one of the higher shells. On the basis of a comparison of the calculated transition energies with the measured peak energies, it was concluded that all of the observed groups correspond to transitions from initial states formed by $2p \rightarrow 3s$ (group A), $2p \rightarrow 3p$ (group B), $2p \rightarrow 3d$ (group C), and $2p \rightarrow 4d$ (group D) excitation to the final state $(1s^2 2s^2 2p^6)\,^1S_0$.

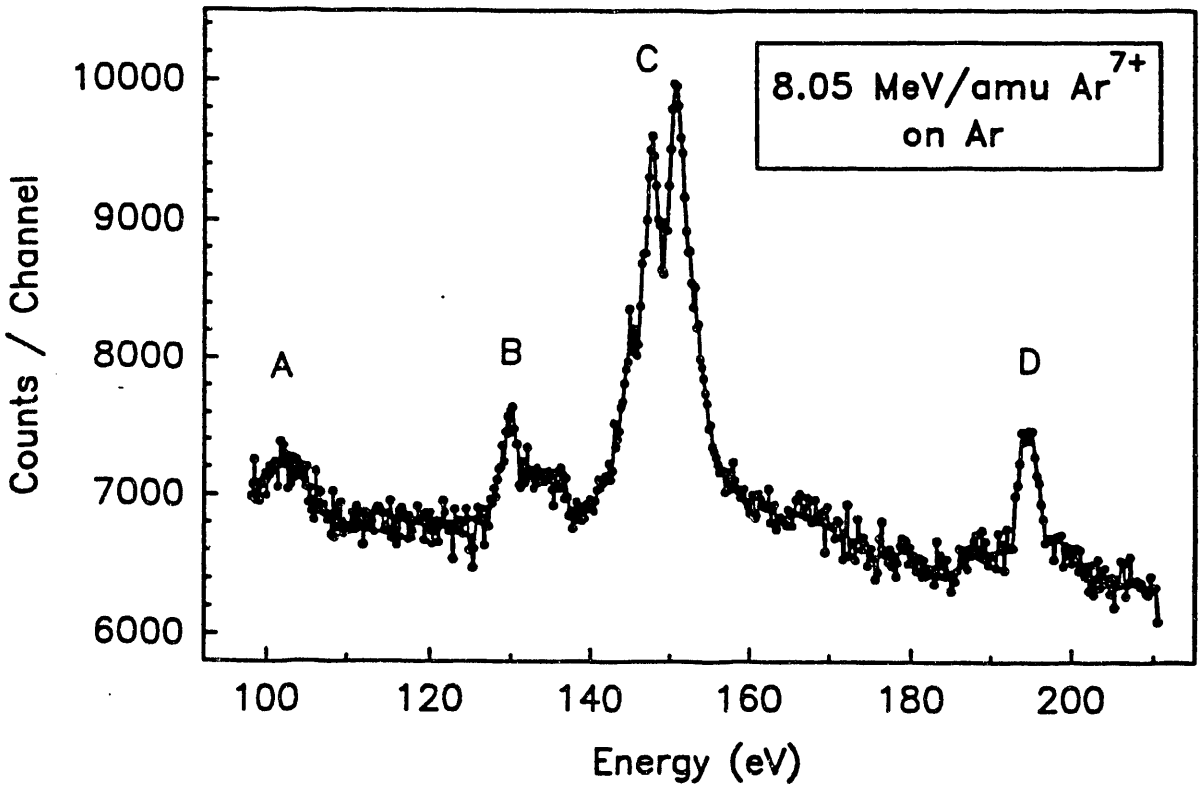

Figure 3. Spectrum of L-Auger electrons from 8 MeV/amu Ar^{7+} measured at 180^{o}.

The peak widths in the laboratory frame are larger than those in the projectile rest frame due to the kinematic stretching effect [3]. This effectively enhances the resolution of the spectrometer. On the other hand, the lines are broadened due to the finite acceptance solid angle of the spectrometer and the variation of the laboratory energy with observation angle. The latter effect dominated in the present case and hence transitions between individual multiplet states could not be fully resolved. The production cross section for the most prominent peak in group C was estimated to be of the order of 1 kb.

Collaborators from Battelle Pacific Northwest Laboratories, Richland, WA

* Collaborator from Lawrence Livermore Laboratory, Livermore, CA

REFERENCES:

[1] D. Bruch, N. Stolterfoht, S. Datz, P. D. Miller, P. L. Pepmiller, Y. Yamazaki, H. F. Krause, and J. K. Swenson, Phys. Rev. A35, 4114 (1987).

[2] J. P. Descalux, Comp. Phys. Comm. 9, 31 (1975).

[3] N. Stolterfoht, Phys. Rep. 146, 317 (1987).

H. PC-Based Multiparameter Data Acquisition System and Program Package CAMACQ (V. Horvat and R. L. Watson)

A new PC-based data acquisition system has been constructed using CAMAC data processing electronics for use in multiparameter experiments. The advantages of a PC-based multiparameter data acquisition system with customized software are the following:

- the system is always available and remains set up for the needs of the group,
- it is simple to operate,
- it can easily be moved from one experimental area (or lab) to another,
- it can be modified without the aid of computer or software specialists,
- the performance of the system is fully known and predictable,
- the acquisition process can never be unwillingly interrupted or slowed down since there is no time-sharing with competing processes, and therefore the acquisition rate is constant,
- the acquired data can be easily and conveniently stored, retrieved, or transferred to another system if necessary.

On the other hand, the disadvantages of such a system are the following:

- the personal computer is a single process machine; it is not possible (without hardware modifications or complicated machine-language programming) to access the acquired data without

interrupting the acquisition,

- the memory and the direct-access storage space are small compared to the more sophisticated computer systems and memory manipulation operations can in some (rare) cases be complicated.

The above disadvantages of the system, however, impose no serious restraints on the experiments planned for the foreseeable future. The system has been used successfully in several experiments and test measurements, and its performance was found to be satisfactory.

The CAMAC [1] part of the hardware setup consists of a 12-slot, 1510-P1C Powered CAMAC Crate with a 3922-Z1A parallel bus crate controller and a 2926-Z1A IBM PC Interface with direct memory access from Kinetic Systems Corporation (KSC). An Ortec AD811 CAMAC Octal ADC modified to accept a maximum of +8 volts on the input (whereas the standard unit accepts +2 volts), a LeCroy 2551 12-Channel 100 MHz Scaler, and a KSC 3195 6-Channel 16-Bit D/A Converter provide for various forms of data input to the system. It is possible to replace the ADC with a TDC without any additional modifications to the system.

The PC part of the hardware consists of a personal computer (Computer Access CA 386-20) with an 80386-20 MHz processor, an 80387 mathematical coprocessor, 4 Mb RAM, 40 Mb hard disk, two high density floppy disk drives (5.25" and 3.5"), a SyQuest SQ555 high performance removable cartridge disk drive, a 16-bit VGA card, a Logitech series 9 mouse, and an IBM graphics printer. The equipment described above, together with three NIM bins is mounted on a cart that can be easily moved from one place to another.

The software for the data acquisition system (designed and written by V. Horvat) consists of the main program CAMACQ which controls the data acquisition, a set of batch files that control the data file handling, a parameter file, and a set of utility programs for off-line data processing and analysis.

The main program CAMACQ (as well as the other utility programs) was written in Microsoft FORTRAN (Ver. 3.3) using also the KSC CAMAC driver model 6110-1BAP, the KSC library of driver routines, a special library of utility routines, and the Microsoft DOS ANSI.SYS driver. The task of this program is to acquire the data and store them into a data buffer. When the buffer is full, the program temporarily stops the data acquisition and copies the data from the buffer onto a RAM disk. Then it resumes the data acquisition. The program also allows for interrupts during which it is possible to (a) view histograms of the acquired data, (b) issue any CAMAC command, (c) resume the data acquisition process (which is not active during the interrupt) or (d) end the program. Optionally the program controls the data acquisition rate using an internal or external timer. The time and the data buffer size, as well as the quantity of data to be acquired can be preset. The format of the output data can be selected to be binary or formatted. The program can also be set to display the data on the screen as they are being acquired.

While testing the performance of the system it was found that, for some unknown reason, the look-at-me (LAM) signal from the ADC is not a reliable indicator of the presence of data at the output. The LAM signal is set and/or reset falsely in a certain fraction of the ADC

readings, and this fraction increases when the signal rate increases. Due to these false LAM signals the data were read, in some cases, only partially, and, in most cases, without some of the least significant bits. This reduced the resolution of the spectra and increased the noise. To overcome this difficulty, a special algorithm was developed for accurately reading the ADC output. This eliminated the problem completely.

The program requests an itemized description of the measurement and writes this information to the parameter file. In the next run, the program reads the description information from the parameter file and allows the user to either accept it as is or to change it, thereby keeping the information up to date without excessive typing. The description of the measurement together with all the steps performed by the program during the acquisition (due to internal causes or user actions), along with the clock times at which they occurred are written into a log file.

The batch files and a few small auxiliary programs are responsible for naming the files produced by the main program and copying them from RAM disk to either the fixed or the removable disk. It is also possible to write the data directly to the disk during data acquisition.

The utility programs perform the following functions:

- displays histograms of the data acquired previously in one- and two-dimensional form,
- selects the acquired data from the event-by-event file and changes the data format (if desired),

- merges histograms and event-by-event files,
- exports/imports files from/to the Nucleus PCA program for single-parameter data acquisition and analysis,
- analyzes the data by applying linear or nonlinear fitting algorithms using up to ten Gaussians with exponential tails and/or step functions, and a polynomial background of up to the ninth degree. The parameters of the fitting function may be fixed, variable, or linearly dependent on one another.

Among the utility programs, the peak fitting program is the most sophisticated. It reads the data directly from histogram (graphics) files, smoothes the data, and calculates the statistical weights. Equal weights or Poisson weights can be selected. The region of interest can have fixed limits or variable limits that are calculated from the peak centroids and widths. Marquardt's method [2] is utilized in the nonlinear fitting procedure. The resulting optimal fitting parameters and the fitting function, along with the other data that describe the quality of the fit, are given in the output description file and are also graphically presented in a file which has the same format as the input file. All the files involved are ASCII files.

The optional scaler in the system is controlled by the main program and is used to measure singles counting rates of the signals. It can also be used to measure the coincidence rate. With this information, the acceptance efficiency of the multiparameter data acquisition system can be calculated. It can also be used in conjunction with a fixed-frequency pulser, to provide an external clock for more accurate

estimates of the count rates. The main program reads the scalers on a regular basis, writes the readings in a separate log file, and displays the count rates of the signals from all the active channels. In addition, a separate utility program was written to display the number of counts in all the active channels simultaneously on the computer screen and to provide standard functions such as preset count/time, start, stop, reset, and freeze display. The program also displays the current and cumulative count rates of the signals in all active channels, monitors for excessive fluctuations in the count rates, and allows the user (while in the stop mode) to issue any CAMAC command to the system. At the end of a run, the program prepares a report containing the measurement identification text, the total numbers of counts (up to 20 decimal digits), and the minimum, maximum, and average count rates. The CAMAC D/A converter is currently used in the system to gate other PCs used as pulse-height analyzers, so that singles spectra can be accumulated simultaneously with the coincidence spectra during exactly the same time intervals. In the near future it is planned to use the six-channel D/A converter to control the voltages of a parallel plate electron spectrometer in measurements of Auger electron spectra.

References

[1] CAMAC Instrumentation and Interface Standards, IEEE, New York, NY, 1982.

[2] D. W. Marquardt, J. Soc. Ind. Appl. Math. 11, 431 (1963).

I. PC-Based Electron Spectrometer Control System and Program ESCAM

(V. Horvat)

An electron spectrometer control and data acquisition system was designed to automate the operation of the tandem-type, parallel-plate, zero-degree electron spectrometer, to process the signals from detectors, and to perform rudimentary data analysis operations. The system utilizes a CAMAC interface and a personal computer. The basic hardware consists of a Kinetic System Corporation (KSC) CAMAC crate, a KSC 3933 Parallel Bus Camac Crate Controller that controls the operation of CAMAC-type electronic modules, and a KSC 2926-Z1A IBM PC Interface W/DMA card that enables communication between the personal computer and the crate controller.

As shown in the schematic diagram in Figure 1, the electron spectrometer consists of two parallel-plate capacitors. The role of the first set of plates is to deflect the electrons from the beam path without affecting the beam. Due to its large apertures, the energy range of the deflected electrons is quite broad and the transmission is very high. The second set of parallel plates analyzes the energy of the incoming electrons in high resolution at the cost of significantly reduced transmission. The design and operation of the electron spectrometer has been described in detail in Refs. [1] and [2].

The entrance plate of the first stage of the spectrometer is normally operated at ground potential and voltages are applied to the other three plates of the system. These voltages are denoted HV(T), HV(B), and HV(D) in Figure 1, where T, B, and D stand for the top, bottom, and decelerating plate, respectively. If a channeltron

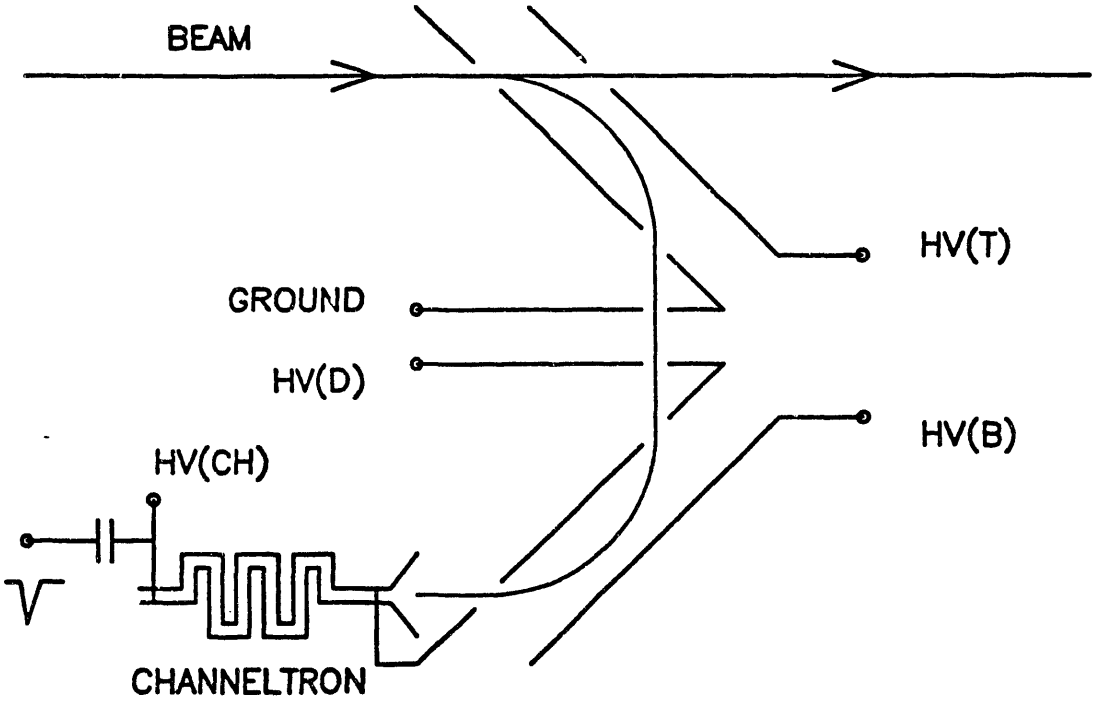

Figure 1. Schematic diagram of the tandem-type, parallel plate, zero-degree electron spectrometer.

electron multiplier is used to detect the electrons emerging from the spectrometer (as in the present application), it is advantageous from the standpoint of background reduction to maintain the front at voltage HV(D) and supply an additional voltage HV(CH) to the back. All the voltages mentioned above depend on the energy of the electrons being transmitted through the spectrometer and the desired resolution. When the spectrometer is scanned to accumulate an electron spectrum, these voltages must be stepped up and down over the appropriate voltage intervals.

One of the functions of the spectrometer control system is to automate the voltage stepping cycles. This is accomplished by using a KSC 3195 6-channel, 16-bit, CAMAC digital-to analog converter (DAC) to provide control voltages to a set of programmable high voltage power

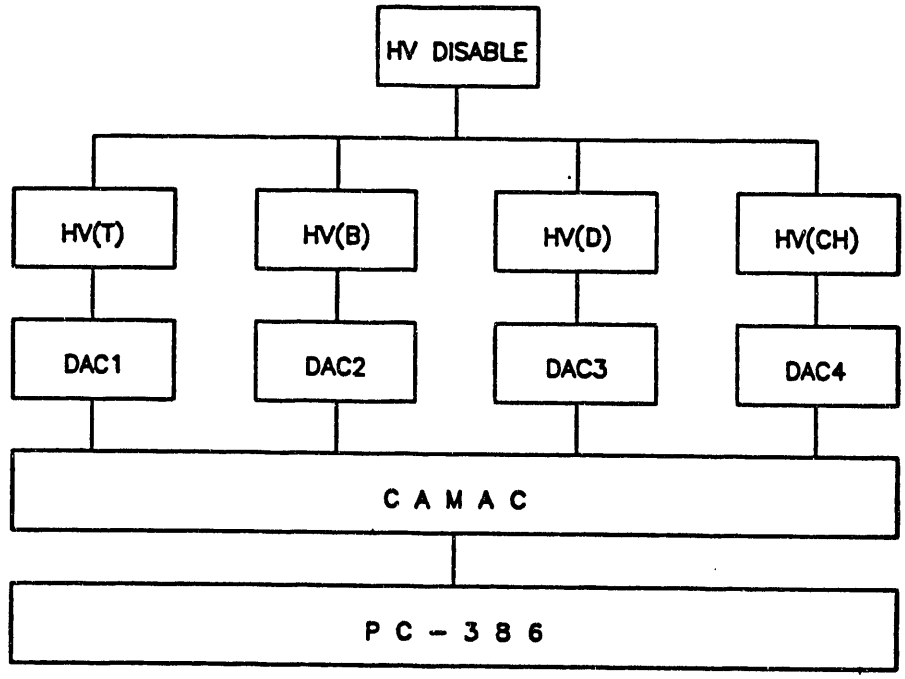

Figure 2. Schematic diagram of the spectrometer voltage control system.

supplies (TENNELEC TC 952), as shown schematically in Figure 2. The voltage provided by each power supply is the sum of the manual dial setting (offset) and the input (DAC) control voltage multiplied by a preset gain factor of 100 or 300. Also, the voltage may be removed remotely by grounding the disable input.

A schematic diagram of the signal-processing part of the system is shown in Figure. 3. Signals from a 60 Hz pulser are sent to channel 1 of a Lecroy Research Systems (LRS) 2551 12-channel scaler and used to measure the live time of the system. The signals from the channeltron electron multiplier (CHAN) are sent through a Canberra 2003B preamplifier (PA) to an Ortec 571 Spectroscopy Amplifier (A), converted into logic signals using a timing single-channel analyzer (TSA) and counted by channel 2 of the scaler.

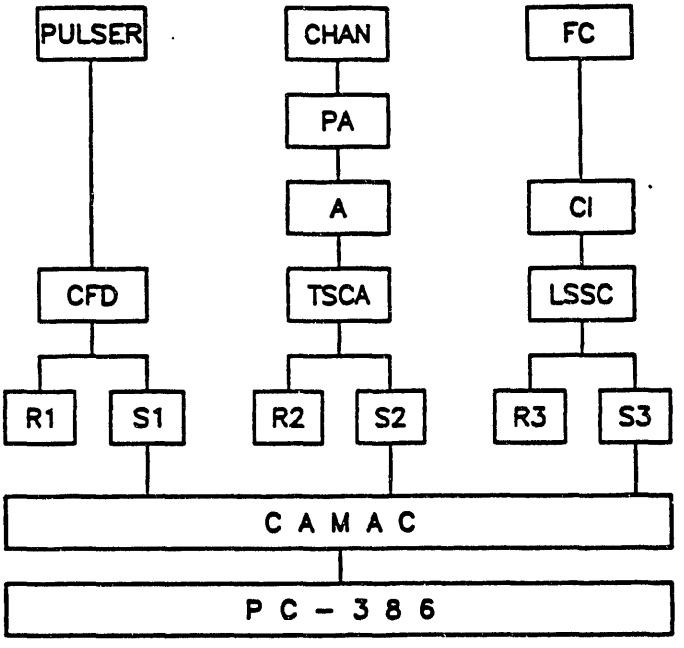

Figure 3. Schematic diagram of the signal processing system.

A Faraday cup (FC) is normally placed behind the detector in measurements with particle beams to provide normalization for the voltage scan counting intervals. The FC current is integrated using a Brookhaven Instruments Corporation (BIC) Current Integrator (CI). The signals from the CI are sent through a logic signal shape converter (LSSC) to channel 3 of the scaler.

The software for the acquisition and control system consists of the program ESCAM and a package of programs for displaying, plotting, and analyzing the acquired data, and for file conversions. ESCAM was written in Microsoft FORTRAN (Ver. 3.3) using also the KSC Camac Driver model 6110-1BAP, the KSC library of driver routines, and a special utility routine library. The positions of CAMAC modules in the CAMAC crate, and their characteristics are defined in a configuration file so that these can be changed without having to change the program

itself. The program provides for the automated fine adjustment of the voltages that are applied to the spectrometer during the scan cycles after fine adjustment of the starting voltages has been performed manually. The required voltages on the spectrometer are calculated automatically, depending on the desired resolution (high or low), the spectrometer constant, the electron energy range, the pass energy, and the selected power supply gain factor. A warning sound is made if the gain factor needs to be changed.

The program ESCAM is designed to minimize the amount of input required from the operator, to be simple to use, and to document all the operator initiated actions. After the first session, in which pre-defined default values of the parameters are assumed, the default values are automatically updated to the ones used in the preceding session. Selection of each menu item is logged and date/time stamped. The current sweep, current live time, and real time (in seconds clocked from the beginning of the session) are logged as well. The same logging procedure is enacted when preset count or preset time conditions are met, or when the acquisition is terminated by the operator. The values of all relevant parameters (including the accumulated spectra) are kept on the hard disk to reduce the risk of loosing data due to power failure, program bugs, or inappropriate usage. In most of the cases of abnormal termination of the program (such as those resulting from power failure, calculational or input/output error, or invoking ^C), it is possible to restart ESCAM with a minimum loss of data and/or other information.

The program ESCAM traps most of the input errors and handles them

without abnormal termination. Usually, re-entering the input or typing ^Z will correct the problem. The message DISK WRITE ERROR will be reported and program execution stopped if the disk on which a write was attempted did not have enough space available. However, no data will be lost, so that after some cleaning of the disk space it will be possible to resume program execution.

Except when the input parameters need to be entered, the up-to-date spectrum graph, and the values of all the control parameters that define it are shown on the screen with a resolution of 320x200 pixels. The flow of the program is menu-driven and the selection is made by pressing the appropriate (pre-defined) easy-to-remember "active" keys on the alphanumeric keyboard. Low graphics resolution and keyboard input were chosen to avoid unnecessary hardware dependability of the program and to increase the speed of operation and execution.

The data acquisition can be either stopped immediately or at the end of the current sweep. It will stop automatically if the preset counts or preset time condition is met. In that case, the preset values will be automatically incremented by the initial values to enable continuation of the data acquisition. During data acquisition, one of the program options enables the time period between successive events in the FC scaler to be continuously monitored and a warning to the operator generated whenever the period exceeds the selected time duration. Exit from the program is possible at any time without any loss of data or information, since before exiting all the data are automatically stored onto the disk and read later when the program is restarted.

REFERENCES

[1] G. A. Harrower, Rev. Sci. Instr. 26, 850 (1955).

[2] A. Itoh, T. Schneider, G. Schiwietz, Z. Roller,H. Platten, G. Nolte, D. Schneider, and N. Stolterfoht, J. Phys. B16, 3965 (1983).

VI. APPENDIX

Reprints of publications resulting from this grant since the last reporting period.

Reprints removed & cycled separately.

END

DATE FILMED

4/20/93